Astrophysical S-factor calculation for selected reactions

Universidad de los Andes
Colombia

Author:
Carlos Alberto Calvachi Salas
201822667

Final project submitted in partial fulfillment of the requirements for the degree of

Physicist

Advisor:
Neelima Govind Kelkar Ph.D.

Abstract

Review on relevant elements of nuclear astrophysics.

Definition, motivation and applications of the astrophysical S-factor.

Survey on models that predict S-factors. They are mainly classified as empirical, potential, macroscopic and matrix models

Use of theoretical models to calculate the S-factors of selected reactions.

Comment on the applicability of the models for each reaction. Comparison between experimental data and theoretical predictions of the S-factors.

Acknowledgments

Mom for everything.

Contents

List of Figures

List of Tables

Chapter 1

Nuclear astrophysics fundamentals

In order to apply nuclear astrophysics to the study of star element production, there are essentials to be considered. In this chapter, a general review of the main points relevant for nuclear physics are presented that emphasizes selected topics that are relevant in the field of nuclear astrophysics.

1.1   General aspects about the nucleus

Introduce a brief description of the nuclei. The structure of the nuclei The nuclear models
The nucleus is a bound state of a system of protons and neutrons. These substructures are bound states of a set of fundamental particles, which are called quarks.

A general treatment given in [1] and basic concepts in [2].

A more particular on nuclear astrophysics [3].

Rest energy.

$$E_0 = Zm_pc^2 + (A - Z)m_nc^2 - B(A, Z), \tag{1.1}$$

where Z, A are the atomic and mass number respectively.
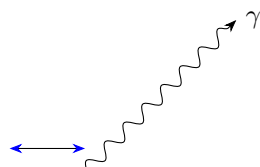
In addition,
Elementary nuclear structure - Atomic nuclei are bond states of nucleons They are particles Characteristics - They obey the Pauli-exclusion principle like electrons - They have magnetic moment. - They are bonded in the nuclei by the strong force which compensates the repulsive electromagnetic force - Each nucleon is conformed by elementary particles. Classification - proton: positive charge - neutron: no charge
- Mass number. Atomic number.
Leptons Characteristics - They do not interact via strong force - Considerably lighter in mass than nucleons Classification - Electron - Neutrino - Antiparticles are also considered

1.2 Elements of quantum mechanics for nuclear physics

Quantum mechanics governs the physics at the nuclear scale. In particular, some elements of quantum mechanics theory that are essential for the description of nuclear reactions. For instance, quantum mechanical treatment of scattering theory is critical for determining the behavior of the rates of the reaction. In addition, tunneling phenomena, which can only be explained from the non-classical behavior of nuclear physics, permits the existence of nuclear fusion. Finally, transition phenomena will be considered in this section from the point of view of electromagnetic transitions.
Quantum mechanics text [4].

1.2.1 Scattering theory

Explain scattering theory relevant for the understanding of processes.

The sequence of the calculations on scattering is the following - Consider free path approximation -> Bessel Function solution - Expand free wave in terms of Bessel and Harmonic oscillator solutions - Obtain the coefficients of the expansion - Evaluate asymptotic behaviour at $r \to \infty$
When considering a potential, it appears that the oscillatory asymptotic wave function is shifted $e^{2i\delta_l}$. This factor depends on the angular momentum l. This directly relates with differential cross sections.

A reference text on collision theory [5].

$$\sigma = \frac{\text{scattered per time}}{(\text{incident per time per area})(\text{total nuclei})}. \tag{1.2}$$

Cross sections are probabilities The probabilities are ruled by the laws of scattering theory, which can be understood as a subpart of quantum mechanics.
There is of interest the differential cross section. Particularly, there is a connection with quantum mechanics scattering amplitudes with the formula

$$\frac{d\sigma}{d\Omega} = |f(\theta, \phi)|^2 \tag{1.3}$$

Cross section -> Reciprocal factors -> Scattering potentials -> Coloumb Barrier (With WKB approximation) -> Breit - Weigner formula (This is for resonant behavior)-> S factors, ...

There are several contributions to the total rate. There are four in principal Broad resonances, thin resonances, continuum, nonresonant. For particles of matter, the statistics at the star fusing scale is Maxwell - Boltzmann and for photons the Bose - Einstein statistics.

Scattering theory develops from the method of partial waves. It roughly consists on solving for the Schödinger equation in free space and, with the potential given, expand in terms of an orthonormal basis of functions, like spherical Bessel and Neumann functions and spherical harmonics. Then, conditions are adjusted via boundary condition satisfying.

$$\psi = \sum_l \sum_m c_{lm} Y_m^l j_l(kr) \tag{1.4}$$

Wavefunction ansatz

$$\psi = \frac{u}{r} Y \otimes \chi. \tag{1.5}$$

Free space solution with $j_l(kr)$ the spherical Bessel function of l parameter. There are also the $n_l(kr)$ Neumann function and the Hankel functions $h^{(1)}(kr)$ and $h^{(2)}(kr)$ functions.

A result that relates cross sections and the probability current density is the theorem.

$$\sigma = \frac{4\pi}{k}\text{Im}(f(\theta = 0))) \tag{1.6}$$

Born approximation that is used for estimating the scattering amplitude.

$$f(\theta) = -\frac{2m}{\hbar^2}\int_0^\infty \mathcal{F}\{V(r)\}dk. \tag{1.7}$$

1.2.2   Tunneling phenomena

Quantum tunneling phenomena is critical in understanding the phenomena of alpha particles decaying in the nuclei barriers.
WKB approximation for the classical forbidden regions.

$$T = e^{2i\delta_l}. \tag{1.8}$$

Ansatz:

$$\Psi(r) = \Psi_0 \exp\left(\Phi(r)\right). \tag{1.9}$$

The Schrödinger equation transforms as

$$\left(\Phi'' + \Phi'^2\right)\Phi = \left(\frac{2m}{\hbar^2}(U(r) - E)\right)\Phi. \tag{1.10}$$

Then, if it is considered that $\Phi'' \ll \Phi'^2$, then Φ can be directly integrated and is expressed as:

$$\Phi(E) \approx -\frac{1}{\hbar}\int_{r_1}^{r_2}\sqrt{2m(U(r) - E)}dr, \tag{1.11}$$

where r_1 and r_2 correspond to the lower and higher classical turning points respectively. In this opportunity, the negative choice for the square root was taken in order to account for the fact that the probability of transmission decreases within the non-classical region.
More information in [6].

1.2.3   Perturbation theory

Generalities of perturbation theory. Cross sections. Fermi Golden rules.

$$\sigma \propto |\langle k|\delta H|m\rangle|^2 \tag{1.12}$$

Splitting

$$m_l = -1$$

$$l = 1 \qquad\qquad m_l = 0$$

$$m_l = 1$$
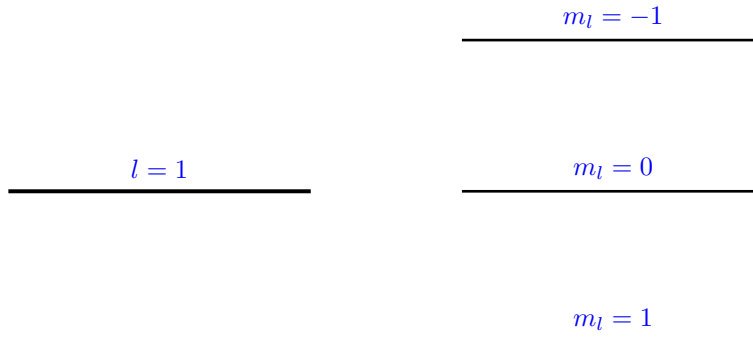
The changes of state that nuclei exhibit obey certain rules. In particular, this selection rules consider angular momentum conservation.
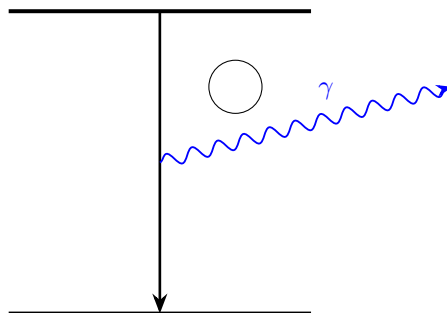
Selection rules. Electromagnetic interaction and resonances [7].

1.2.4 Angular momentum

1.3 Nuclear structure

Nuclear structure is presented in this section.

1.3.1 Nuclear models

Stability depends closely on the biding energy. In particular, since the rest energy of the nucleus decreases with $B(A, Z)$, the more is the binding energy, the more stable is nucleus.

Liquid drop model

A first approach when modeling the binding energy is a phenomenological model which is inspired in the physical description of a liquid drop. In particular, the predictions of the binding energies are determined by the fitting of the empirical formula:

$$B(Z, A) = a_v A - a_s A^{2/3} - a_3 \frac{Z(Z+1)}{A^{1/3}} + a_4 (Z - A)^2 + a_5 \delta. \tag{1.13}$$

However, this model does not fit accurately the binding energy of a selected nuclei which are more stable than expected from the model. In particular, it is said that the pair of number of protons and nucleons (Z, A) of these nuclei are magic numbers.
- The more stable the nuclei, the greater the binding energy. Binding energy is the energy difference of rest energy of the nucleus constituents and the actual rest mass of the overall nucleus.

$$\delta = \begin{cases} 1, & Z \text{ and } A \text{ even} \\ -1, & Z \text{ and } A \text{ odd} \\ 0, & \text{otherwise} \end{cases} \tag{1.14}$$

Nuclear shell model

An alternative approach to the Liquid drop model is a model based on quantum mechanics. This model is closely related with the quantum mechanical modeling of the hydrogen atom. In particular, a great part of the nuclear shell model consists of solving Schrodinger equation which is expressed as:

$$-\frac{\hbar^2}{2m}\partial_{tt}\psi + V\psi = E\psi. \tag{1.15}$$

In this case, the potential V represents the effective potential of the core of the nucleus and is valid at certain radii. For example, the harmonic potential $V = m\omega^2 r^2$ models effectively the system of nucleons at most regimes.

Spin orbit coupling rules the energy levels of the nucleons.

- Nuclear shell model is based on quantum mechanics.
-Nuclear shell model can predict the existence of the magic numbers.

$n = 5$ ————————

$n = 4$ ————————

$n = 3$ ————————

$n = 2$ ————————

$n = 1$ ————————
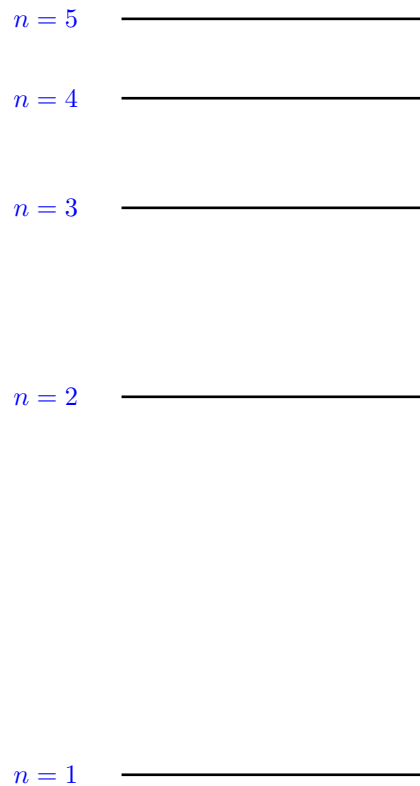
1.3.2   Nuclear levels and transitions

1.4   Nuclear reactions

Nuclear reactions are reactions between nuclei. [8].

^{2}H

^{1}H

^{3}He

^{2}H ^{4}He ^{3}H

^{1}H
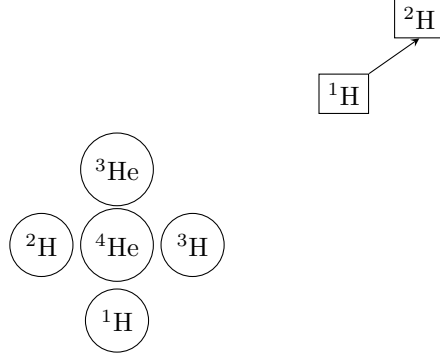
1.4.1 Classification of reactions

The relevant reactions for the document are:

$$0 + 1 \rightarrow 2 + 3 \tag{1.16}$$

$$\gamma + 3 \rightarrow 0 + 1 \tag{1.17}$$

Expand on how the fusion reactions occurs, their conditions and types as well as the differentiation factors with respect to fission processes.

Capture reactions

Also, radiative capture processes are considered at astrophysical energies. Various models could be used for determining potentials. There are clusters and potential models.

$$X + c \rightarrow \gamma + X'. \tag{1.18}$$

When c is a proton, the reaction is called radiative proton capture. [9]

Exchange reactions

$$X + x_1 \rightarrow x_2 + X' \tag{1.19}$$

A development on the (p, n) reaction kind is given by [10] and for the (n, p) in [11].

Fusion reactions

$$X + X \rightarrow a + X'. \tag{1.20}$$

1.4.2 Cross sections

Cross section of a process. Partial and total cross sections depending on the reaction type. Cross sections have relations with the S-matrix.

1.4.3   Reaction rates

The ratio that determines the quantity of a nucleus.

$$r = A \int_0^\infty E\sigma(E) \exp\left(-\frac{E}{kT}\right) dE. \tag{1.21}$$

$$P(v)dv \propto v^2 \exp\left(\frac{mv^2}{2kT}\right) dv. \tag{1.22}$$

On specifying the rates, it is needed to be considered.
Reaction rates are considered from calculation of transmitted, incident and interacting - Reaction rate depends on the density of particles, the velocity and the cross section - It is averaged by a convenient distribution. (Maxwell-Boltzman for fermions, Bose Einstein (Planck) for photons) - With the rates, abundance evolution is determined
There are broad classification of reactions.

1.5   The Astrophysical S-factor

1.5.1   Motivation and definition

There are S factors associated with the energy and they are the path to determine the nature of the potential, which is not necessarily a Yukawa potential.

$$S(E) = E \exp(2\pi\eta)\sigma(E). \tag{1.23}$$

It is directly proportional to the microscopic cross section of the process $\sigma(E)$ and it represents the rate of a certain nuclear reaction. In particular, the astrophysical S-factor scales the cross section with a factor proportional to the Coloumb repulsion.
The ν factor is defined as

$$\eta = \frac{Z_1 Z_2 e^2}{4\pi\epsilon_0 \hbar v} \tag{1.24}$$

where v corresponds to the relative speed between the reactants.
There is a strong relation of the astrophysical S factor with the center of mass energy.
Usually this relation depends on the square of the energy of the center of mass E_{cm}.

There are topics that are relevant in the frontiers of nuclear astrophysics [12].

1.5.2   General applications

Cross section extrapolation to low energies
Reaction rates and element abundance estimations.

Chapter 2

Reactions of astrophysical interest

Nuclear reactions are part of the core of nuclear astrophysics. They are accountable for the mechanism of production of elements in several astrophysical environments where thermonuclear reactions occur. In particular, there are specially relevant reactions for the explanation of the abundance of elements. For example, some of these reactions are part of critical fusion chains of stars, have challenging extrapolation techniques to low energies, or exhibit exotic underling physical phenomena. In this section, a relevant selection of reactions types of will be reviewed.

Several reaction kinds and models are given in [13].
Screening effect present in light weight nuclear reactions [14] and a review of screening effect [15].

2.1 Big bang nucleosynthesis

Primordial reactions that where expected to happen after the big bang occurred. For example:

$$^2\text{H} + \text{p} \rightarrow \gamma + {}^3\text{H}. \tag{2.1}$$

2.2 Stellar fusion

The classical treatment of fusion in stars is given by the classical [16].
Introduce the needed conditions for the creation of stars in the primordial nebula. Describe how the hydrogen is burnt in the star's core and the associated products.

$$p + p \rightarrow d + e^+ + \nu_e. \tag{2.2}$$

Consider the mechanisms for exchanging heat via radiation and convection.
Explain the required conditions that permits nuclear fusion in the star's nucleus.

2.2.1 Light heavy nuclei reactions

This reaction is governed by the weak force, due to conversion of a proton into a neutron, and by the strong and electromagnetic force.
When it comes to deuterium fusion, this channel is the most abundant.

$$d + d \rightarrow n + {}^3\text{He}. \tag{2.3}$$

The reaction rates of nuclear fusion processes depend on the interaction cross section and the abundance of the reactant nuclei.

$$d + d \rightarrow p + t. \tag{2.4}$$

The interactions of the previous processes are the electromagnetic and strong force.

$$^3\text{He} + p \rightarrow {}^4\text{Li} + \gamma \rightarrow {}^4\text{He} + e^+ + \nu_e + \gamma. \tag{2.5}$$
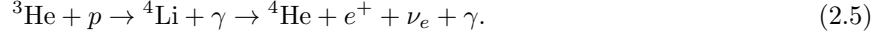
This process is unlikely because of the instability of ^4Li, which decay to ^3He.

$$^3\text{He} + {}^3\text{He} \rightarrow {}^4\text{He} + 2p. \tag{2.6}$$

This process in known as the pp1 chain.
Exemplify how the reaction mechanisms permits the stability of a star as well as produces He.

2.2.2   CNO cycle

The carbon burning produces the neutrons that are going to be used in heavy nuclei production. The neon burning stats by fusion Neon nuclei with 4He nuclei to produce heavier elements. The oxygen burning starts are very high temperatures and pressures than the neon and carbon burning due to the high stability of oxygen nuclei. In fact, oxygen nucleus is double magic.

When the star has capacity for producing elements like carbon, oxygen and nitrogen, CNO cycle process can be produced. In particular, reactions take the form

$$^{12}_{6}\text{C} \rightarrow {}^{13}_{7}\text{N} \rightarrow {}^{13}_{6}\text{C} \rightarrow {}^{14}_{7}\text{N} \rightarrow {}^{15}_{8}\text{O} \rightarrow {}^{15}_{7}\text{N} \rightarrow {}^{12}_{6}\text{C}. \tag{2.7}$$
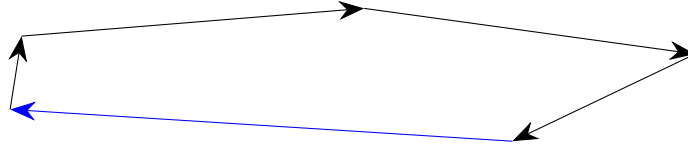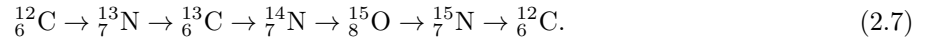
There are other CNO cycles that involve oxygen and fluorine reactions. For instance, the second CNO cycle consists of the following reactions

$$^{15}_{7}\text{N} \rightarrow {}^{16}_{8}\text{O} \rightarrow {}^{17}_{9}\text{F} \rightarrow {}^{17}_{8}\text{O} \rightarrow {}^{14}_{7}\text{N} \rightarrow {}^{15}_{8}\text{O} \rightarrow {}^{15}_{7}\text{N}. \tag{2.8}$$
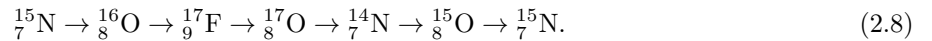
There is even a CNO III cycle, which is far more uncommon. brig This branch is less dominant than the first branch.

2.2.3   Medium heavy fusion reactions

These reactions concern nuclei with $A < 28$. Examples of this kind of reaction include the $^{12}\text{C} + {}^{12}\text{C}$, $^{12}\text{C} + {}^{16}\text{O}$ and the $^{16}\text{O} + {}^{16}\text{O}$ fusion reactions. Most of these reactions result in different channels.

With respect to the carbon fusion reaction, the principal channel is given by:

$$^{12}\text{C} + {}^{12}\text{C} \rightarrow {}^4\text{He} + {}^{20}\text{Ne}. \tag{2.9}$$

On the other hand, the main channel of the oxygen fusion reaction occurs in the following manner:

$$^{16}\text{O} + {}^{16}\text{O} \rightarrow {}^4\text{He} + {}^{28}\text{Si}. \tag{2.10}$$

Additionally, there are inelastic channels associated with ^{16}O which could increase the probability of occurrence for the overall reactions.

$$\alpha + {}^{28}\text{Si}$$

$$\alpha + {}^{20}\text{Ne}$$

$$p + {}^{31}\text{P}$$

$$p + {}^{23}\text{Na}$$

$$^{16}\text{O} + {}^{16}\text{O} \longrightarrow d + {}^{30}\text{P}$$

$$^{12}\text{C} + {}^{12}\text{C} \longrightarrow d + {}^{22}\text{Na}$$

$$\alpha\alpha + {}^{30}\text{P}$$

$$\alpha\alpha + {}^{16}\text{O}$$

$$n + {}^{31}\text{S}$$

$$n + {}^{23}\text{Mg}$$
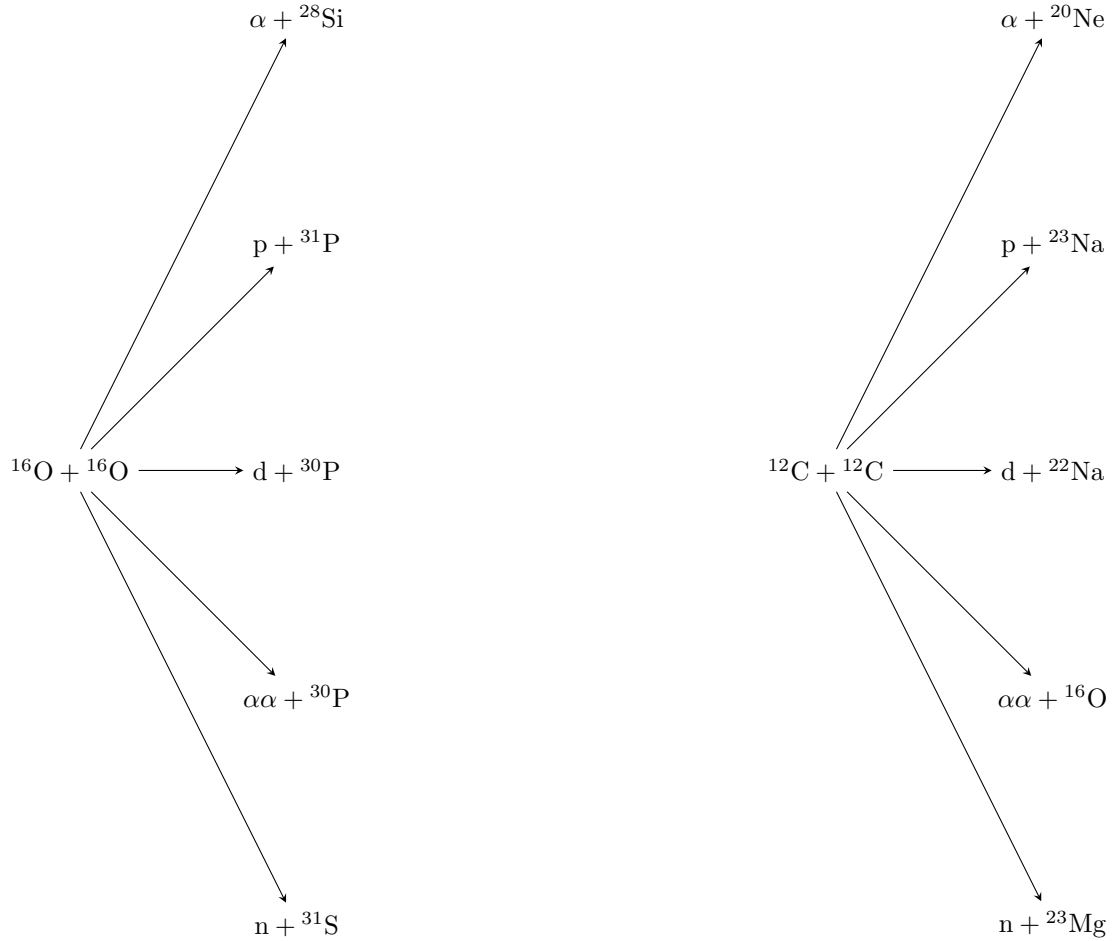
There are more cycles of capture reaction. An example regarding the MgAl cycle is given in [17].

Explain the different chains going on during the carbon-oxygen combustion to heavier elements like iron or silicon.

The Trojan horse method[18]

nucleosynthesis in massive stars [19]

12C + 12C Wave packet dynamics[20] nonresonant Bayersian [21] Modified sfactor [22] Trojan horse [23] [24] full-microscopical [25] multichannel folding [26] screening effects [27]

correlation between carbon fusion reactions [28] constraint 12C + 12C based on 12C + 13C reaction [29]

16O + 16O cross sections [30] [31]

oxygen isotopes fusion [32] coupled channels [33]

12C + 16O semi-microscopic cluster [34] low-energy resonances [35] 12C + 16O based on yields of 12C + 16O and 12C + 18O [36]

selected oxygen-oxygen and oxygen-carbon reactions [37] [38] 12C + 12C and 16O + 16O [39]

12C and 24 Mg resonances [40] Fusion hidrance 12C + 24Mg [41]

heavy-ion reactions [42]

2.3 Supernovae and other explosive environments

Additional fusion reactions with nuclei with $A > 28$ are present at the last stages of the life of a star. There are two main environments: The stellar fusion and explosive events fusion.

2.3.1 Heavy nuclei reactions

There is a silicon burning process with the following description

$$\ce{^{28}_{14}Si} + \ce{^{4}_{2}He} \rightarrow \ce{^{32}_{16}S}. \tag{2.11}$$

Silicon burning is another process.

$$\ce{^{28}Si} + \ce{^{28}Si} \rightarrow \ce{^{4}He} + \ce{^{56}Fe}. \tag{2.12}$$

This reaction is essential since the ^{56}Fe nucleus has the maximum binding energy. Then, fusion reactions of heavier nuclei tend to be less spontaneous.Then, this chain of reactions continues until the process in there 56-Ni is reached.

$$\ce{^{52}_{26}Fe} + \ce{^{4}_{2}He} \rightarrow \ce{^{56}_{28}Ni}. \tag{2.13}$$

2.3.2 The s and r processes

There exists the s and the r processes. Each permits to form heavier nuclear elements products. Now, there are aspects of the particularities of the production of the nuclei that are currently unknown

On the other hand, protons are captured at the ending of the life of a gigantic star. This process, which occurs at high densities and temperatures, is referred as proton capture. In particular, under astrophysical scenarios like supernovas, the rapid proton capture, in addition to the neutron capture, produces a considerable amount of the heavy nuclei. This process is referred as rapid proton capture, or rp process.

Further processes are not viable because they are not exothermic and potential heavier nuclei than 56-Ni are photodisintegrated. At this scale of energy, nuclear reactions start to behave similarly than chemical equilibrium reactions.
The conditions are associated with the mass. Particularly, depending on the mass regime, star evolution can differentiate. For instance, there are brown dwarfs, sun like stars.

There is an evolution process that is ruled by different instances. Each instance can be regarded as a region in the Hertzsprung-Russell diagram. This diagram consists of a two dimensional scatter plot of the intensity with respect to the spectral type of a star. Particularly, there are regions associated to the different instances of the life of a star: Main sequence (Hydrogen burning stars), red stars, neutron stars, supernova of kinds Ia Ib and other instances.

Electron degeneracy prevents the white dwarf to collapse and the neutron degeneracy pressure prevents the neutron star to collapse. These limits account for relativistic Fermi gas and neutron degeneracy with a model from general relativity.

Indicate that there exists different channels of production depending on the existence of neutron capture or fission products. Additionally, explain the needed conditions in order to those processes to occur.

If mass increases further, there is no place to any degeneracy compensation so the star would collapse to a black hole.

2.3.3 The p and sp processes

2.4 Active research topics

Enumerate the broad ranges of phenomena that are left to be explained.

Introduce current approaches of some of the unsolved questions on nuclear astrophysics, particularly on the last instances of fusion in the star's lifetime.

There are various types of supernovae. However, there are mechanisms that are not considered and yet not well explained.

Current experiments in detection of heavy nuclei are essential to determine the distribution of elements, specially in events like the fusion of neutron stars.

Review on active research topics and current challenges in nuclear astrophysics in general [43] and on low-energy nuclear physics [44] are given.

Chapter 3

Astrophysical S-factor models

There are several methods for estimating the astrophysical S-factor. Each method is more convenient depending on the nature of the reaction. For example, method accuracy can vary depending on the reaction type or the existence of resonant phenomena. Additionally, the methods are based on a specific approach when modeling the S-factors. In this section, the principal methods of estimating the astrophysical S-factors will be reviewed.

3.1 Microscopic models

Microscopic models are based on first principles and usually require assumptions about the nucleus and its structure.

$$H = \sum_k T_k + \sum_k V_k(r) + \sum_{k \neq j} V_{kj}(r). \tag{3.1}$$

Modern theories [47]

3.1.1 *Ab initio* models

Stats from first principles without prior empirical or phenomenological assumptions.
Ab initio [49] [50] [51] [52] tensor force [53]

3.1.2 Many body models

Non-local calculations. Multi-body calculations.

Also, nuclei deformation can be considered in models. For example, there are models with no-core shell.

Three body [48]
No core shell model [54]
Hauser-Feshbach [61]
Hartree-Fock [64]

3.1.3 Cluster models

On the other, clusters consider the system of interactant nuclei as a whole. In particular, there are models based on *ab initio* assumptions about a particular set of nuclei.

NN and NNN interactions.
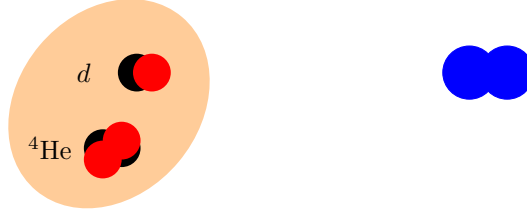
The *ab initio* no core shell model is presented in [45].

A more detailed survey on cluster models [46].

$$\int \int \rho(r_1)\rho(r_2)dr_1dr_2. \tag{3.2}$$

The mass and nuclear density of the nuclei can be modeled as:

$$\rho(r) = \frac{\rho_0}{1 + \exp\left(\frac{r-R}{a}\right)}. \tag{3.3}$$

Shell model [55] [56]
Multicluster [59] [60]
Break up effects [62]
Linear chain [63]

3.2 Matrix models

The matrix models permit the modeling of resonances with an appropriate fitting of free parameters. In particular, the main formalism in this approach is the R-matrix model [65] [66].

On the other hand, there are matrix models with no free parameters. For example, the K-matrix model predicts the cross sections without including the channel radius, which is an arbitrary parameter required in the R-matrix calculations [84].

Finally, there is more than a single parametrization for matrix models [85]. Usually the alternative formulations surge from the need to express the parameters of the model in order to facilitate the imposition of boundary conditions.

3.2.1 Calculable R-matrix

The model includes free parameter a which is called the radius channel.

$$R_{cc'} = \sum_k \frac{\gamma_{ck}\gamma_{c'k}}{E - E_k}. \tag{3.4}$$

The sum is over levels and the elements are parameterized as channels.

Resonances arrives from poles. A description on the physical consideration of poles in the scattering (S-matrix) is given in [67].

Applications of the R-matrix formalism to specific reactions:

In primordial nucleosynthesis [68] big-bang 3He and several reactions [69].

Bayesian fitting methods [70].
Litium detueron capture [71].

10B proton non-radiative [72] and similarly [73]. 10B radiative and resonances in 11C inverse kinematics [74].
Alpha capture reactions of carbon [75]. Hybrid potential/R-matrix [76].
13C alpha capture and 16O determination [77].
Proton capture carbon [78] for C12 and [79] for C13 and [80] for the same reaction .

15N capture in [81] and 14N in [82]. also on 14N proton capture [83].

3.2.2 Phenomenological R-matrix

The penetration factor parameter $P(E)$ which is expressed as:

$$P = \frac{\Gamma}{F_l^2 + G_l^2},\tag{3.5}$$

where the functions $F_l = F_l(ka)$ and $G_l = G_l(ka)$ are the Coulomb functions evaluated at a particular $\rho = ka$. In addition, another parameter Q is given:

$$Q = \frac{\Gamma}{F_l G_l' + G_l F_l'}.\tag{3.6}$$

On the other hand, the phase shift is given by:

$$\delta = \delta_{\text{HS}} + \delta_R.\tag{3.7}$$

An empirical formula obtained from the R-matrix formalism is given by:

$$S(E) = S_r \frac{\Gamma^2/4}{(E - E_r + \Delta)^2 + (\Gamma/2)^2}.\tag{3.8}$$

3.2.3 K-matrix

There is also the K-matrix model as an alternative of the R-matrix model [84]. The advantage of this model with respect to the R-matrix is that the K-matrix does not include the channel radius as a free parameter. Alternative formulation of R-matrix [85].

3.3 Potential models

Nuclei are considered as objects subject to effective interactions. These interactions are also modeled by effective potentials which account qualitatively for the nature of the underlying physics behind the nuclear reactions. In particular, different kind of potentials offer a particular shape of the interaction which make them suitable for the modeling of concrete reactions.

3.3.1 Effective potentials

The effective interaction between nuclei is referred as a composite effect of the electromagnetic and nuclear interactions.

The first interaction is considered due to the electromagnetic repulsion between the nuclei. In a first approach, the substructure of the nuclei is ignored. Then, nuceli charged cloud is modeled as uniformly charged sphere. Therefore, the corresponding potential is given by:

$$V_{\mathrm{EM}} = \begin{cases} \dfrac{Z_1 Z_2 e^2}{4\pi\epsilon_0 R}\left(\dfrac{3}{2} - \dfrac{r^2}{2R^2}\right), & r \leq R \\[3mm] \dfrac{Z_1 Z_2 e^2}{4\pi\epsilon_0 r}, & r > R \end{cases} \tag{3.9}$$

Secondly, in order to account for the nuclear force, an short-distance attractive potential is needed to be included. However, unlike the electromagnetic interaction, nuclear potentials might not be deduced in a closed and fundamental form such as the expression given in 3.9. Consequently, these potentials are usually phenomenological and account for specific purposes. In fact, there is a an extent list of potentials available in literature which are used for modeling the interactions of different kind of reactions.

For instance, in a first approximation, there is the step potential.

$$V_{\mathrm{SqW}} = -V_0\theta(r). \tag{3.10}$$

Yakovlev et. al model [86] consists of an estimation of the potential that is similar to the parabolic potentials with free parameters that attempt to account for the effects of the nuclear and electromagnetic interactions.

$$V_{\mathrm{YAK}} = \begin{cases} E_c\left(3 - \dfrac{r^2}{R_c^2}\right), & r \leq R_{c1} \\[3mm] \dfrac{Z_1 Z_2 e^2}{r}, & r > R_{c1} \end{cases} \tag{3.11}$$

Additionally, the model distinguish between classical allowed and forbidden regions. For the first region, where $E < E_c$, the astrophysical S-factor is estimated as:

$$S(E) = S(0)\sqrt{\frac{Ec}{E}}[\exp\left(\Psi(E)\right) + k\xi], \tag{3.12}$$

where ξ is a free parameter of the model that accounts for the deviation from free particle behaviour of the S-factor. On the other hand, $S(0)$ corresponds to the zero-energy extrapolation of the S-factor.

uses the WKB approximation for estimating the wave function. Then, the astrophysical S-factor is determined by a phenomenological equation.

$$\Psi(E) = 2\pi\eta(E) + \Phi(E), \tag{3.13}$$

where $\eta(E)$ is the Sommerfeld parameter, and $\Phi(E)$ is the wavefunction calculated by the WKB. Further details on the calculation of the last parameter are presented in section 1.2.2.

In order to the potential to be more realistic, a Woods-Saxon potential consider a smooth behavior.

$$V_{\mathrm{WS}}(r) = \frac{V_0}{1 + \exp\left(\frac{r-R}{a}\right)}, \tag{3.14}$$

where V_0 represents the potential depth, a the parametrization and R a computed radius which is defined as:

$$R = r_0(A_1^{1/3} + A_2^{1/3}). \tag{3.15}$$

24

On the other hand, it is relevant, specially at low energies, the inclusion of angular momentum effects in the potential. In order to account for that effect, there is the potential with angular moment.

Also, spin orbit coupling effect is noticeable for certain kind of reactions. The contribution to the potential associated with this effect is expressed as:

$$V_{\text{SO}}(r) = k \langle L \cdot S \rangle \frac{1}{m_\pi r} \frac{d}{dr} V(r), \tag{3.16}$$

where the coupling $\langle L \cdot S \rangle$ is expressed as:

$$\langle L \cdot S \rangle = J(J+1) - l(l+1) - s(l+1). \tag{3.17}$$

In the radiative capture reactions, cross sections are computed based on electromagnetic field operators. In particular

$$\sigma_m = \sum_k \langle k | \mathcal{O} | m \rangle C_{klm}. \tag{3.18}$$

Double exponential potentials:

$$V_{\text{DE}}(r) = -V_0 \left(e^{\alpha_1 r} + e^{\alpha_2 r} \right)^{-1}. \tag{3.19}$$

Cluster potential:

$$V_{\text{CL}}(r) = -V_0 \exp\left(-\alpha r^2\right) + V_1 \exp\left(\beta r\right). \tag{3.20}$$

Gaussian exponential:

$$V_{\text{GE}}(r) = -V_0 \exp\left(-\alpha r^2\right). \tag{3.21}$$

Yukawa potential which includes screening effect.

$$V_{\text{Y}} = -\frac{c}{4\pi\epsilon_0} e^{-\mu r}. \tag{3.22}$$

3.3.2 Calculations

The potentials just introduced are useful for the calculation of cross sections and, therefore, S-factors. The connection between potentials and cross sections depends on the kind of reaction to be modeled. In the general approach, cross sections are directly computed form wave functions, which are numerically estimated from the numerical solution of the Schroödinger equation.

On the other hand, in certain specific cases when the expressions of the potentials are not mathematically sophisticated, approximations can be made. In particular, WKB approximation offers a comprehensive approach towards handy estimation of the cross sections.

3.3.3 Folding

During the previous discussion, mass and charge distributions were not considered in detail. However, with nuceli with higher mass, the intrinsic distribution of the mass and charge gains relevance in the reaction cross section estimation. In particular, mass and charge is usually concentrated at the center of the nuceli and there is a sharp drop of the mentioned variables in the surrounding of the radius.

In order to account for this effect, an initial formula which accounts
Sao pablo [98]

$$V_{\mathrm{SPP}}(r) = V_{\mathrm{F}}(r)e^{-4V^2/c^2}. \tag{3.23}$$

$$V^2 = \frac{2}{\mu}\left(E - V_{\mathrm{F}}(r) - V_{\mathrm{C}}(r)\right), \tag{3.24}$$

where the reduced mass is μ, the Coulomb potential is $V_{\mathrm{C}}(r)$ and the folding potential $V_{\mathrm{F}}(r)$ is expressed as:

$$V_{\mathrm{F}}(r) = \int\int \rho_1(\vec{r}_1)\rho_2(\vec{r}_2)\delta(\vec{r} - \vec{r}_1 + \vec{r}_2)d\vec{r}_1 d\vec{r}_2. \tag{3.25}$$
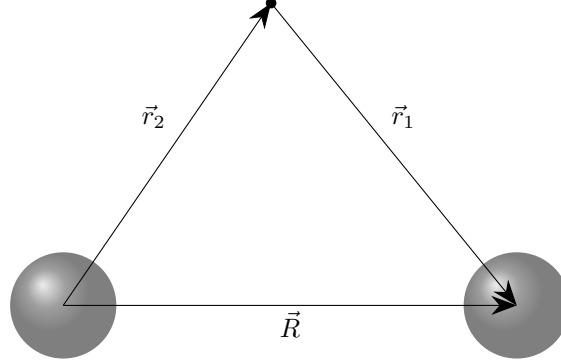
3.3.4 Non-locality

And, potentials with non-locality are also found in literature. For example, there is the São Pablo potential that accounts for the effect of non-local interactions between the interactant nuclei.

Capture reaction review light nuclei[87] [88]
7Be radiative capture [89] [90]
9Be radiative capture [91]
p2H radiative capture [92]
2Hdp reaction [93]
13C radiative capture [94] [95]
11C radiative capture[96]
16O fusion [97]

Optical model [99]

$$V(r) = V_R(r) + iW_R(r). \tag{3.26}$$

Woods-Saxon [100] [101]

$$V_{\mathrm{WS}} = -V_0 f(r), \tag{3.27}$$

$$f(r) = \frac{1}{1 + \exp\left(\frac{r-R}{a}\right)}. \tag{3.28}$$

Energy dependent model [102]
$V_0(E)$
Cross section deduced potential [103] [104]

3.4 Special models

Models which do not fit in the previously presented categories.

3.4.1 Trojan Horse models

It occurs in a two step reaction process as expressed in:

$$A + B \rightarrow a + b \rightarrow a + (c + d), \tag{3.29}$$

where the first and second steps correspond to the $A + B \rightarrow a + b$ and $b \rightarrow c + d$ reactions respectively. Notice that the b nucleus does not appear as a final product of the reaction as it is consumed in the second step.

3.4.2 Effective field theories

Based on effective field theories. The general principle of these theories is that nuclear interactions correspond to low-energy approximate solutions of the physics described in quantum chromodynamics.

$$\mathcal{L} = N^\dagger i\hbar\gamma^\mu \partial_\mu N + ... \tag{3.30}$$

Diagrams associated with the processes of low-energy nuclear force. Mediators are mesons like pions.

Effective field theory [57] [58]

3.4.3 Hybrid models

These models include aspect of potential, microscopical and even R-matrix models. For example, there are models with clustering and effective potentials.

3.5 Empirical formulas

And some empirical formulas can be given.

3.5.1 Interpolations

Non-resonant reactions S-factors can be calculated with polynomial interpolations and fits.
In particular, there is a polynomial expansion that is reported in literature to be useful.

$$S(E) = \exp\left(g_0 + g_1 E + g_2 E^2 + g_3 E^3 + ...\right). \tag{3.31}$$

Also, more generic expansions are modeled by fitting a Laurent series expansion.

$$S(E) = \frac{a_{-1}}{E} + a_0 + a_1 E + a_2 E^2 + ... \ . \tag{3.32}$$

For most of the reactions, $a_{-1} = 0$, since $S(E)$ should be smooth at very low energies. Therefore, the S-factor is described as a Taylor series expansion.

$$S(E) = a_0 + a_1 E + a_2 E^2 + ... \ . \tag{3.33}$$

3.5.2 Fusion reactions formulas

Fusion reactions, which is a more sophisticated model [109].

$$S(E) = \sum_{k=0}^{N} a_k E^k + \left(1 + \exp\left(1 + \frac{E - E_c}{D}\right)\right)^{-1} \sum_{l=0}^{M} b_l E^l. \tag{3.34}$$

3.5.3 Resonances and composite formulas

For resonant reactions, the Breit-Wigner formula

$$S(E) = S_r \frac{\Gamma_r^2/4}{(E - E_r)^2 + (\Gamma_r/2)^2}. \tag{3.35}$$

This formulation permits empirical formulas to add resonant terms to the non-resonant estimation. Usually the resonant terms are added to background which is fitted to a non-resonant formula. For example, consider the expression:

$$S(E) = \sum_{k=0}^{N} a_k E^k + \sum_{l=1}^{M} \frac{\Gamma_l^2/4}{(E - E_l)^2 + \Gamma_l^2/4}, \tag{3.36}$$

Analogously, if the non-resonant term has a polynomial form, the S-factor hybrid resonant and non-resonant expansion is expressed as:

$$S(E) = \exp\left(\sum_{k=0}^{N} a_k E^k\right) + \sum_{l=1}^{M} \frac{\Gamma_l^2/4}{(E - E_l)^2 + \Gamma_l^2/4}, \tag{3.37}$$

where N is the maximum order of the polynomial to be fitted, which accounts for the non-resonant behavior of the reaction, and M represents the number resonances present in the reaction.
Applications in direct capture [105]. Exchange reactions (p, n) kind [106].
Charged particle collisions non-resonant [107] and resonant [108].

Chapter 4

S-factor calculations for selected reactions

In this chapter, the S-factor calculation for a selected list of reactions will be presented. The list of reactions distinguish between resonant and non-resonant reactions. Additionally, this list includes reactions from Big Bang nucleosynthesis, pp-chain, CNO cycle and middle heavy nuclei fusion astrophysical environments.

In order to account for the best predictions for the astrophysical S-factors of the referred reactions, a motivation on the selection of a particular model will be mentioned, as well as the calculation consideration used to perform the calculations will be detailed for each reaction.

Further details about capture reactions with single-particle states is given by [110].

Additional, about pp-chain is given by [111].

Computer libraries that were used:

Python [112], Pandas [113], NumPy [114], SciPy [115], Matplotlib [116].

4.1   Non-resonant reactions

The starting point in the process of analysis of reaction is the study of its non-resonant part.

Light heavy selected reactions are $^2\mathrm{H}(\mathrm{p}, \gamma)^3\mathrm{He}$ and $^2\mathrm{H}(\mathrm{d}, \mathrm{p})^3\mathrm{H}$. On the other hand, $^{12}\mathrm{C} + ^{12}\mathrm{C}$ and $^{16}\mathrm{O} + ^{16}\mathrm{O}$ are the fusion reactions to be considered.

Empirical formulas are initially considered for the light heavy S-factor description. In particular, the non-resonant part of the equations 3.37 and 3.36 are fitted to experimental data.

In addition, a correction factor that accounts for the electron screening effect observed at low-energies in the $^2\mathrm{H}(\mathrm{d}, \mathrm{p})^3\mathrm{H}$ reaction is included.

On the other hand, fusion reactions are described by the Yakovlev et. al empirical formula [109] and potential model [86].

Microscopical and matrix model approaches are used to be describe all the selected reactions.

4.1.1 Calculation considerations

Empirical formulas were determined by fitting parameters to best describe experimental data. In particular, the parameters chosen minimized the chi-squared χ^2 function as it is described in appendix C. In some cases, it was necessary to constraint the interval of validity of the parameters in order to avoid unphysical behaviour of the fittings. Further details about this constraints can be found in section C.1.

For the case of Yakovlev et. al potential model, an analytical calculation was performed. In this calculation, the parameters given in [86] were used for the selected fusion reactions.

In the Yakovlev model, there is a fitting of the parameters in the following way. The free parameters are δ, E_c and ξ. In particular, E_c can be determined by the following expression:

$$E_c = \frac{\alpha}{R}, \tag{4.1}$$

where $\alpha = \sqrt{Z_1 Z_2 e^2}$ and R is a parameter that is determined as:

$$R = R_0 + \Delta R_1 |2Z_1 - A_1| + \Delta R_2 |2Z_2 - A_2|. \tag{4.2}$$

In particular, the parameter R_0 depends on the reactant nuclei while the parameters ΔR_1 and ΔR_2 can assume two values per pair of reactant nuclei. For instance, the values are given in the following way:

$$\Delta R_1 = \begin{cases} \Delta R_{10}, & 2Z_1 > A_1 \\ \Delta R_{11}, & 2Z_1 < A_1 \end{cases} \tag{4.3}$$

Analogously, ΔR_2 is determined as:

$$\Delta R_2 = \begin{cases} \Delta R_{20}, & 2Z_2 > A_2 \\ \Delta R_{21}, & 2Z_2 < A_2 \end{cases} \tag{4.4}$$

The numerical values that were provided in [86] for each of the reactions to be studied are contained in section A.4.

Although Yakovlev et. al model is used for middle-heavy fusion reactions, is not expected to work for radiative capture reactions since it predicts a decrement of the S-factor for all energies. In contrast, the S-factor increases in radiative capture reactions.

4.1.2 Results and analysis

(a) Polynomial fits.

(b) Exponential fits.

(c) Best fits.
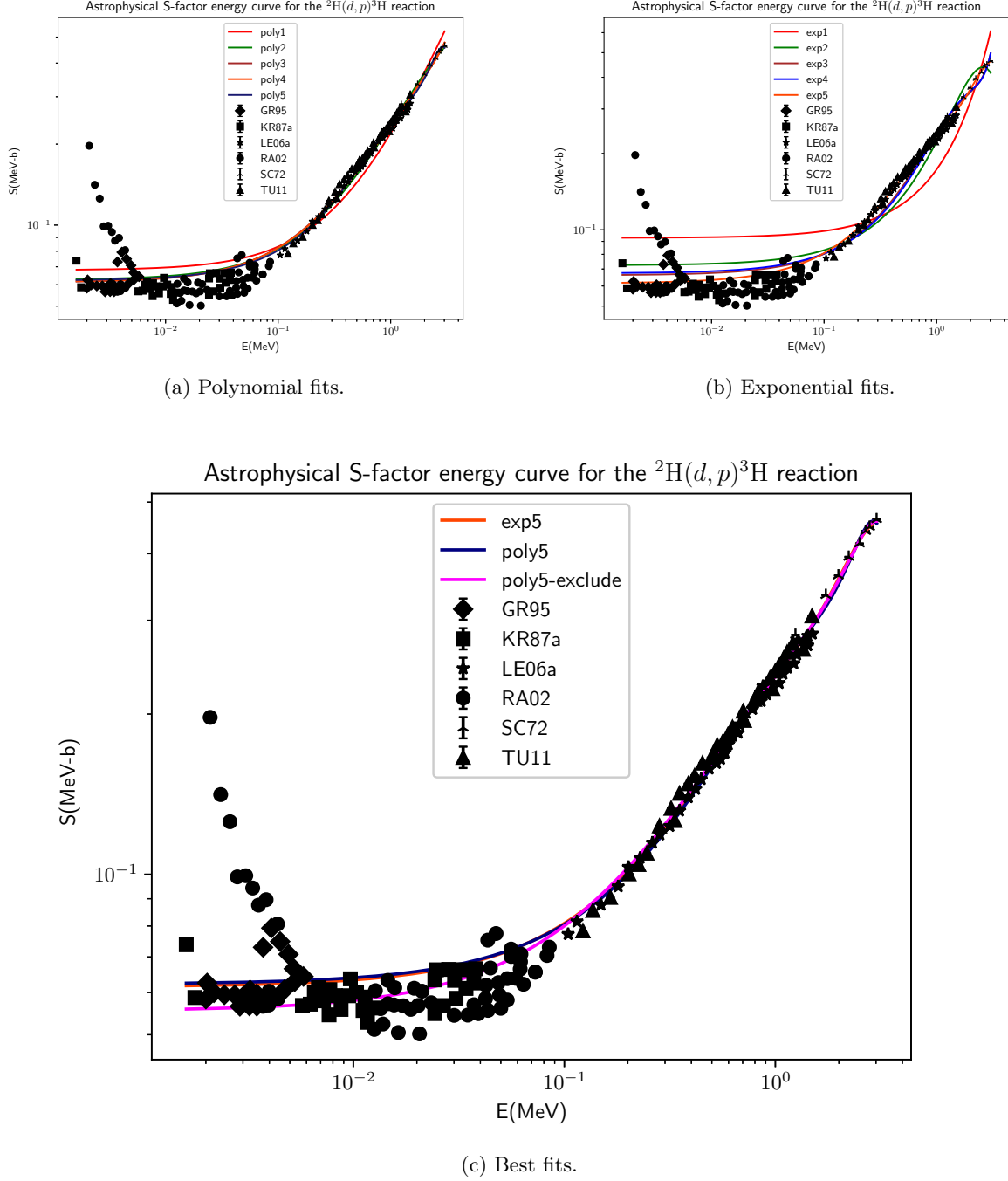
Figure 4.1: Empirical formulas fitted to ^{2}H(d, p)^{3}H reaction S-factor data. In panel a), poly1, poly2, poly3, poly4, and poly5 represent fits to polynomials from 1st to 5th order. Similarly, in panel b), exp1, exp2, exp3, exp4 and exp5 represent exponential fits up to 5th order. Additionally, in panel c), poly5-exclude corresponds to a poly5 fit without data from RA02 and GR95. References to the sources of the black colored experimental points are given in Table A.1. Fitting parameters values are given in Tables C.1 and C.2.

At low-energies as far as 10^{-3} MeV $< E < 10^{-2}$ MeV, an exponential-like damping of the S-factor is observed. In fact, this behavior could explained due to the electron screening effect [14]. In particular, the enhancement factor f for the S-factor is defined as [14]:

$$f = \frac{E}{E + U_e} \exp\left(\frac{\pi\eta U_e}{E}\right), \tag{4.5}$$

where E is the center of mass energy, η is the Sommerfeld parameter and U_e is a parameter that quantifies the degree of enhancement of the S-factor. The sharp increase of the S-factor at low energies is explained by the shielding of the Coulomb potential produced by the electron cloud that surrounds the interacting nuclei [15]. In particular, this dismissal of the strength of the potential reduces the Coluomb barrier. Therefore, as the tunneling probability increases, the cross-section for the reaction also increases.

Additionally, the value of the U_e parameter is usually obtained by fitting. An example of such fitting is found in the graphs of Figure 4.2.
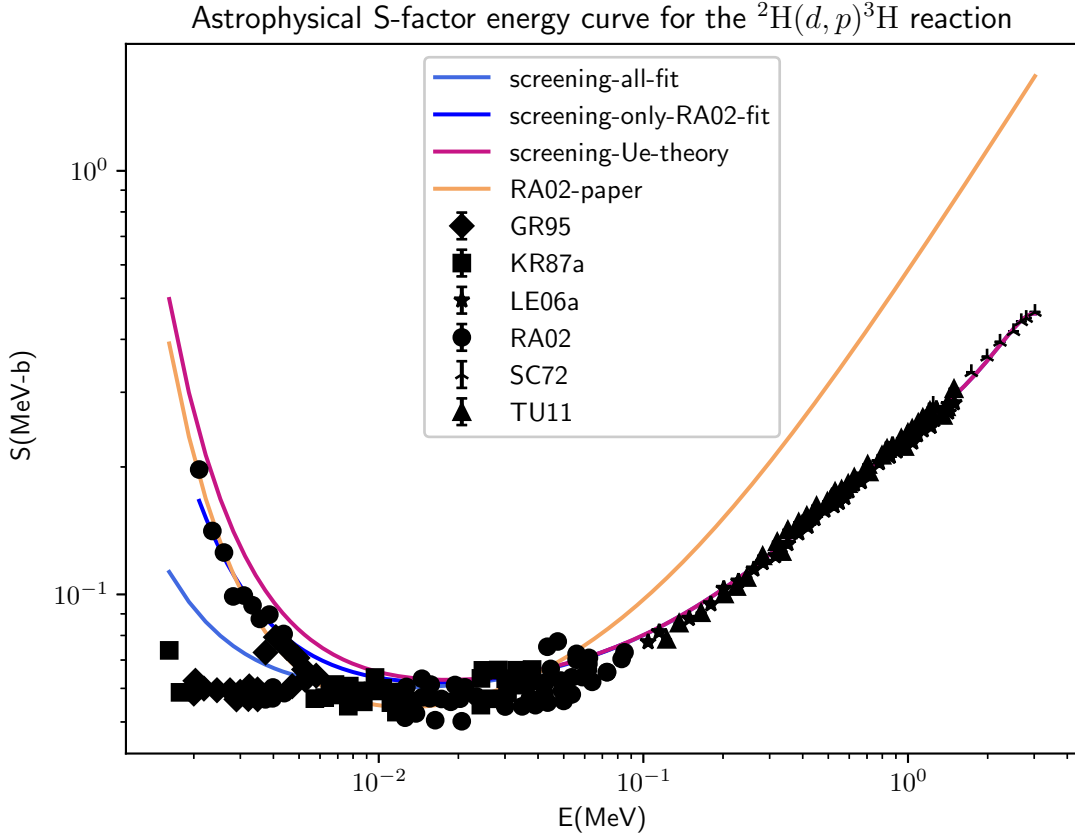
Figure 4.2: Polynomial fits to experimental data with screening effect. The curve labeled as screening-all-fit is obtained by fitting U_e with all data points, screening-only-RA02-fit is obtained only with RA02 data, *screening-Ue-theory* is calculated with U_e fixed to the value given in RA02. The poly5-exclude fit of Figure 4.1 was used as the S-factor estimation without screening of the last three curves. Additionally, the screening-RAO2 curve presents the S-factor prediction made in the RA02 paper. Further details about the fitting parameters and their values are given in Table C.3.

32
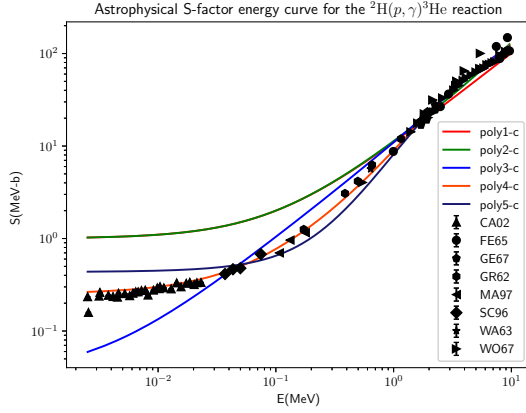
(a) Polynomial fits with constraints.
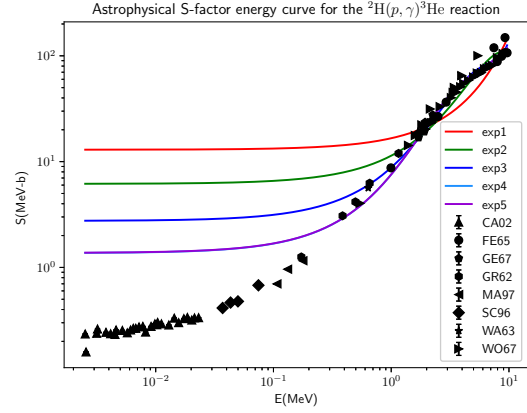
(b) Exponential fits.
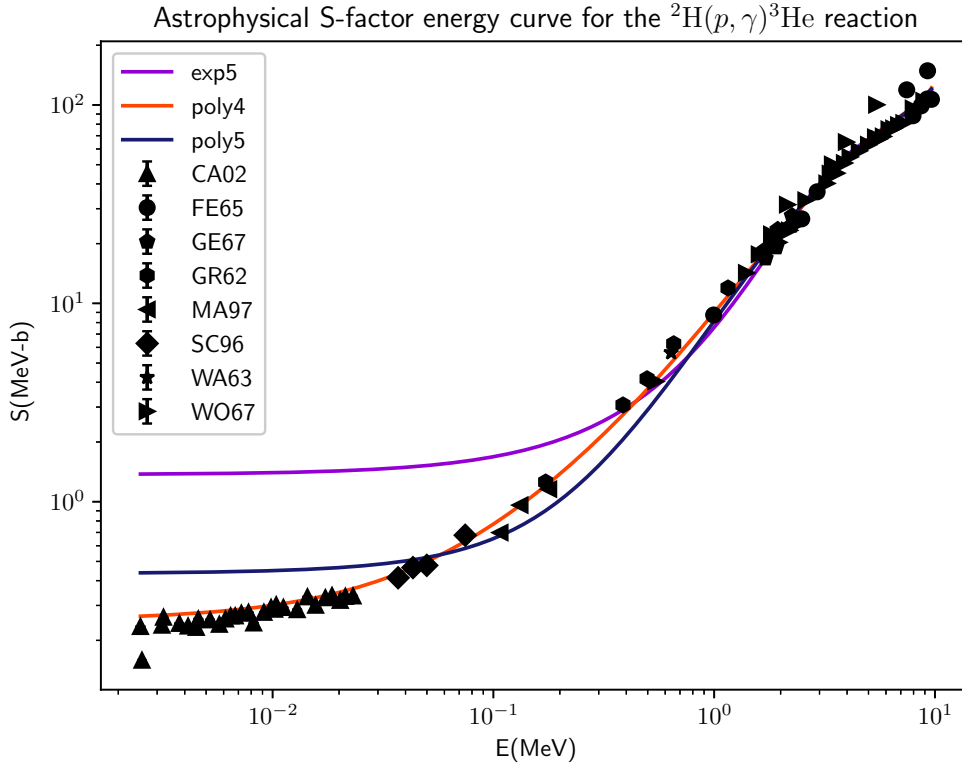
(c) Selected fits.

Figure 4.3: Empirical formulas fitted to the S-factor for the ^{2}H(p, γ)^{3}He reaction. In panels a) and b) polynomial and exponential fits up to fifth order are presented respectively. In particular, the fit parameters used for the graphs in panel a) were constrained. Additionally, in panel c), the best selected fits are visualized. The references to the experimental points are given in Table A.1. The values of the fitting parameters are encountered in Tables C.4 and C.5.

S-factor curve for the low energy regime in Figure 4.3.

Exponential fit does not converge as desired at low-energies.
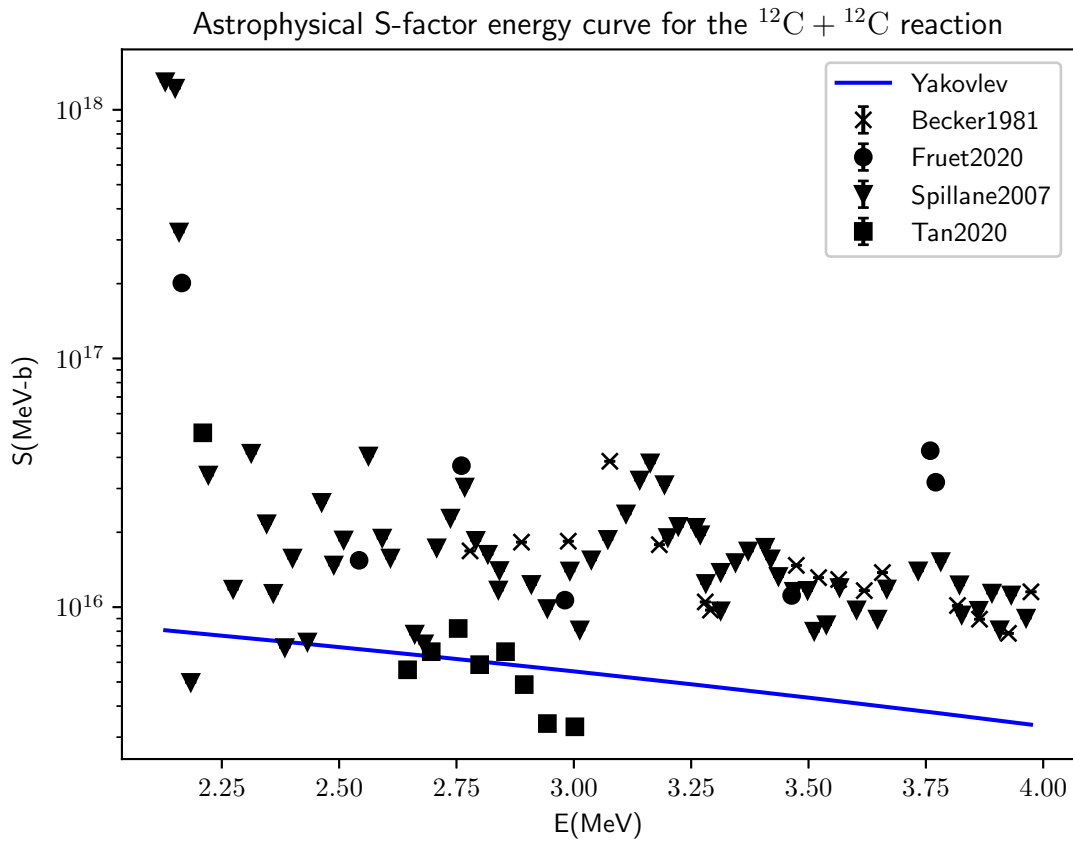
Figure 4.4: Astrophysical S-factor prediction for the $^{12}C + ^{12}C$ reaction as parametrized in the Yakovlev et. al analytical potential model [86]. Experimental points references are presented in Table A.3.
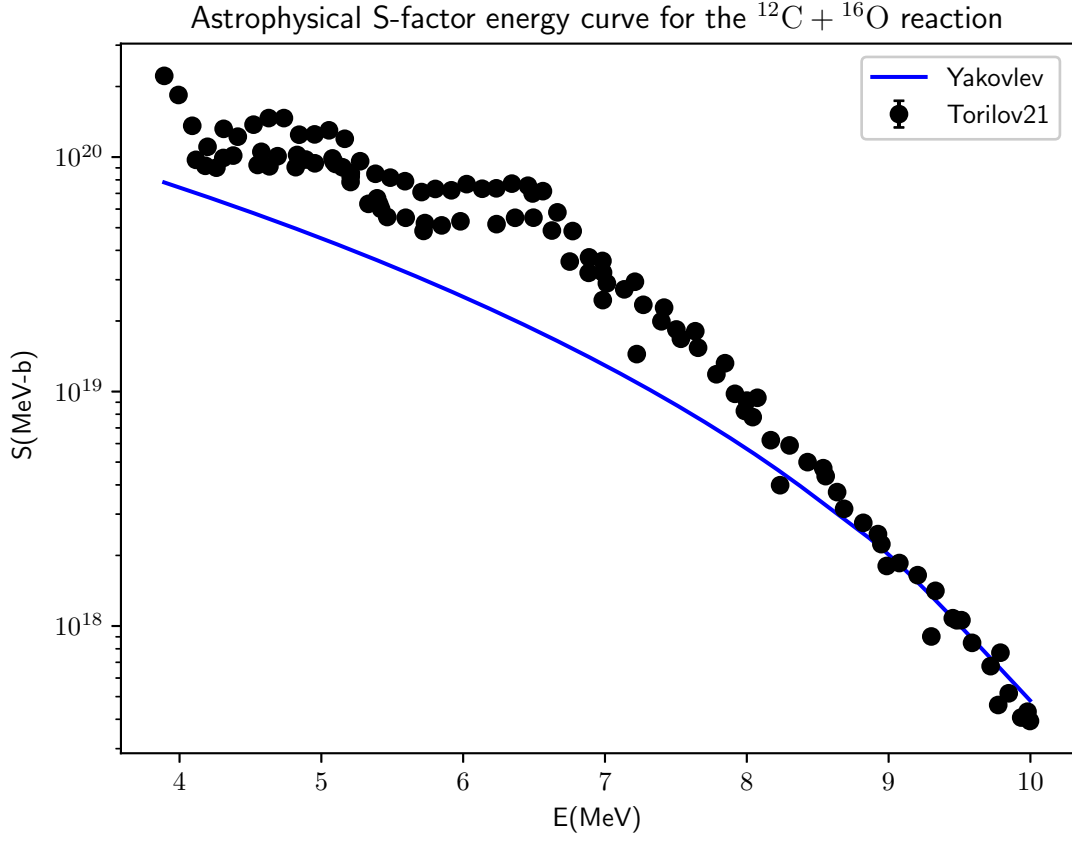
Figure 4.5: Astrophysical S-factor prediction for the ^{12}C + ^{16}O reaction as parametrized in the Yakovlev et. al analytical potential model [86]. The reference for the experimental points is given in Table A.3.
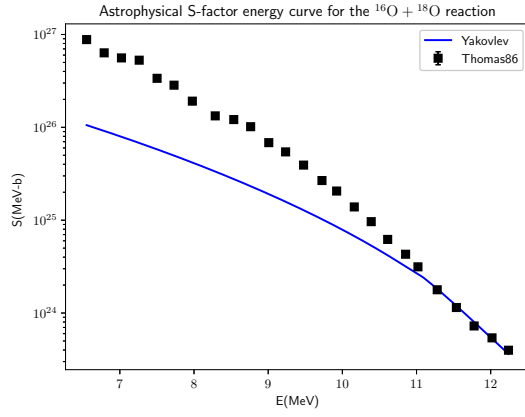
(a) $^{16}O + ^{18}O$ reaction.
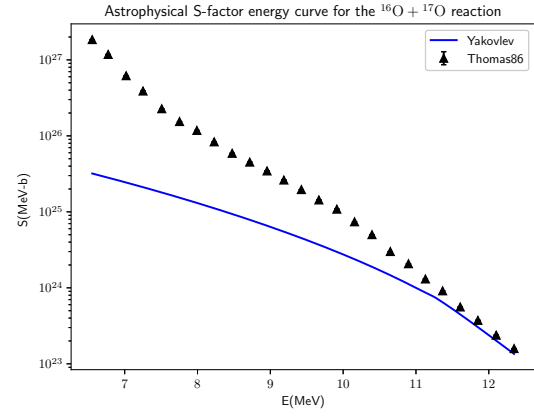
(b) $^{16}O + ^{17}O$ reaction.
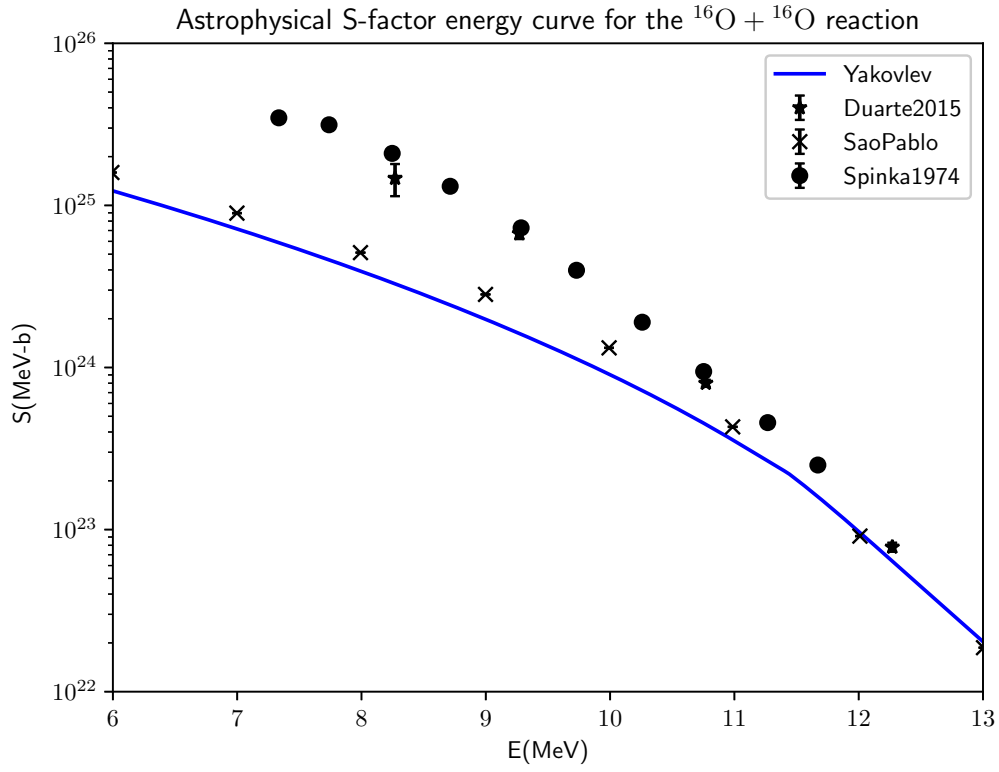
(c) $^{16}O + ^{16}O$ reaction.

Figure 4.6: Potential model prediction for a selection of oxygen fusion reactions. In panels a), b) and c) are presented the Yakovlev et. al prediction for the S-factor of the $^{16}O + ^{18}O$, $^{16}O + ^{17}O$ and $^{16}O + ^{16}O$ reactions respectively. Additionally, in panel c), the *SaoPablo* entry corresponds with the predictions made in [86] which were obtained by using the São Pablo potential model. Experimental data sources are cited in Table A.3.

4.6 4.6c 4.6b 4.6a

4.2 Resonant reactions

It is frequent to find sharp peaks in the S-factor values of some nuclear reactions. The existence of these fluctuations usually suggest the presence of resonant phenomena. In particular, each peak is characterized by additional variables like its height, width and energy center. Then, the non-resonant astrophysical S-factor predictions of section 4.1 shall be modified.

A first apporach towards the description of resonances Breit-Wigner. Single channel approximation.

^{7}Be(p, γ)^{8}B and ^{13}C(p, γ)^{14}N
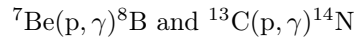
A compilation of additional R-matrix treatment is given by [117].

4.2.1 Calculation considerations

Breit-Wigner empirical formula was used for initial fitting.

4.2.2 Results and analysis

Background estimation with non-resonant fits.
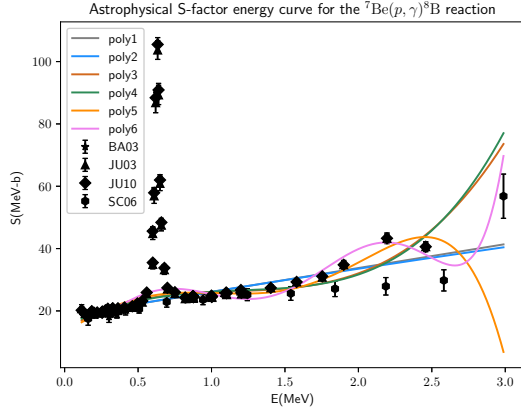
(a) Polynomial fits.
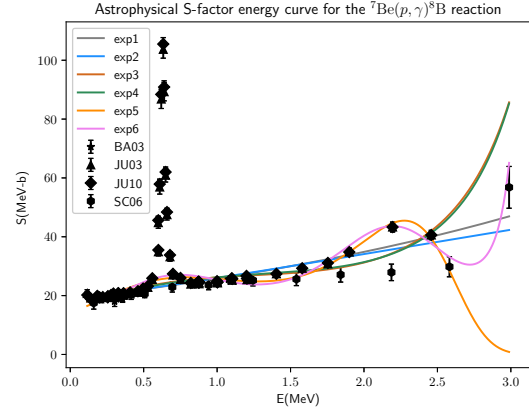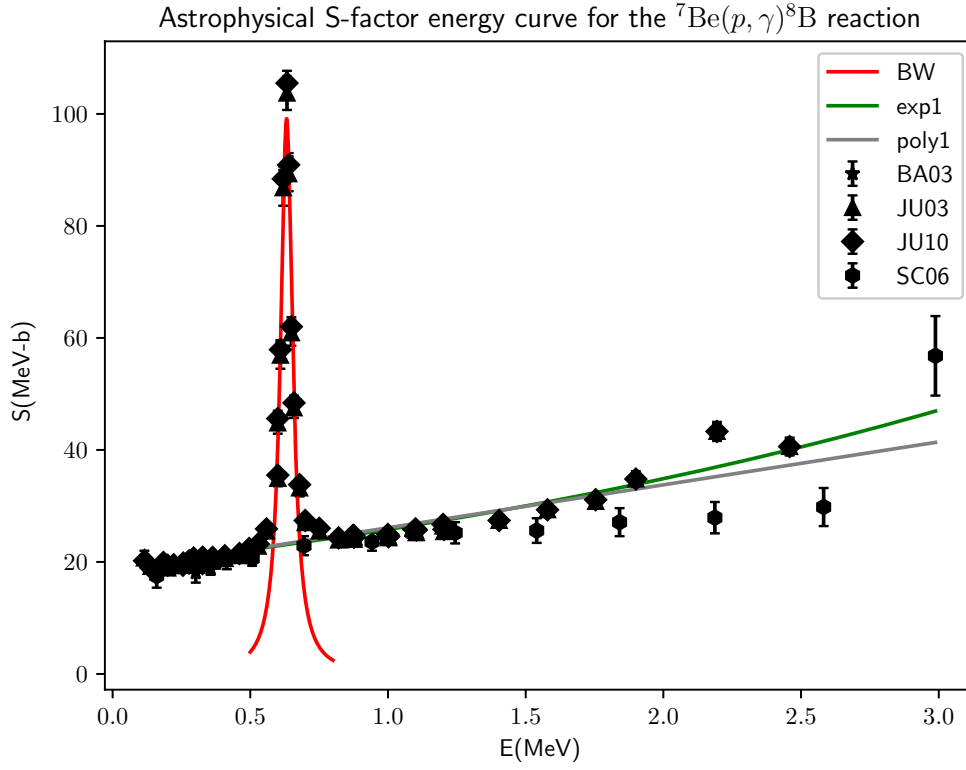
(b) Exponential fits.

(c) Selected fits.

Figure 4.7: Empirical formulas fitted to background of the S-factor for the $^7\text{Be}(p,\gamma)^8\text{B}$ reaction. In panels a) and b) polynomial and exponential fits up to sixth order are presented respectively. Additionally, in panel c), the most simple and accurate fits, in this case exp1 and poly1, were selected. In addition, the BW labeled curve corresponds to a Breit-Wigner fit for the resonance. The references to the experimental points are given in Table A.2. The values of the fitting parameters are found in Tables C.6, C.7 and C.8.
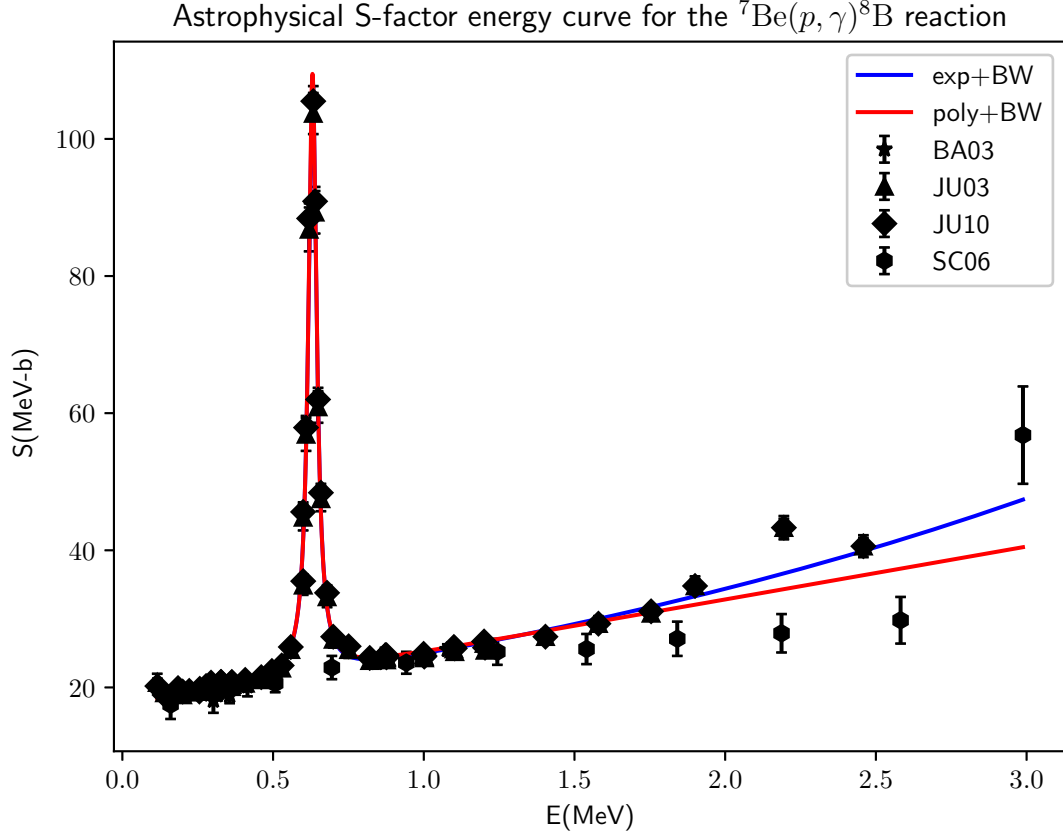
Figure 4.8: Empirical fit for the $^7\mathrm{Be}(\mathrm{p},\gamma)^8\mathrm{B}$ reaction. In this graph, the resonant contribution, as modeled with a Breit-Wigner, was added to the non-resonant background estimation, which was modeled with first order polynomial and exponential formulas. In addition, fitting parameters are found in Table C.9.

A single resonance with a peak close to $E = 0.7$ MeV is observed in Figure 4.8. Then, in order to model the single resonance, a Breit-Wigner fit was performed.

However, as it is visualized in S-factor dependence, this fit does not account for the entire behavior of the experimental points far from the resonance. Consequently, the theoretical prediction is modified to improve the modeling of the non-resonant part of the S-factor.

Additionally, an increment of the background, namely the non-resonant part of the S-factor, is present.
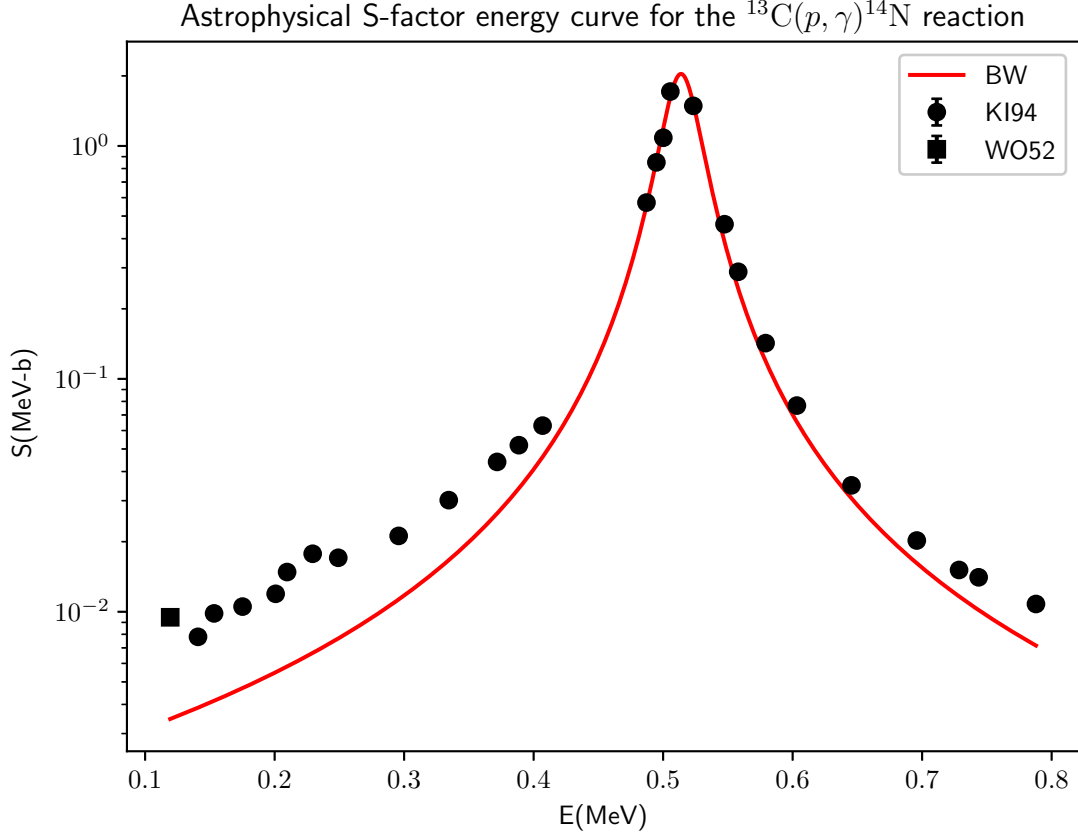
Figure 4.9: Breit-Wigner fit for the S-factor of the resonant $^{13}C(p, \gamma)^{14}N$ reaction. The experimental data points were taken from sources cited in Table A.2. Further details about the fitting parameters and their values are given in Table C.10.

A resonance with a peak close to $E = 0.6$ MeV is observed in the S-factor data presented of Figure 4.9. In order to model this behavior, a Breit-Wigner fit was initially performed.

Despite the global correspondence between the experimental data and the predictions of the fit, the resonant behavior does not entirely explain the shape of the S-factor data. This discrepancy specially occurs far from the resonance peak at low energies. In order to improve the prediction, the non-resonant contribution to the S-factor needs to be included.

In a first approach, the non-resonant background is modeled empirically. In particular, the polynomial and exponential expansion was used.
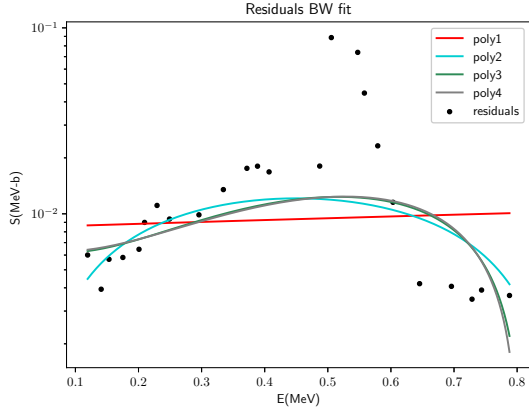
(a) Polynomial fits.
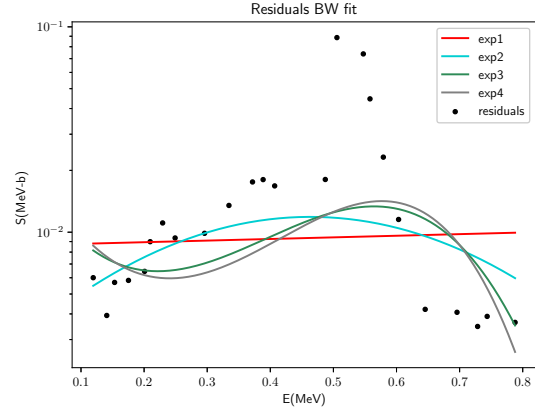
(b) Exponential fits.
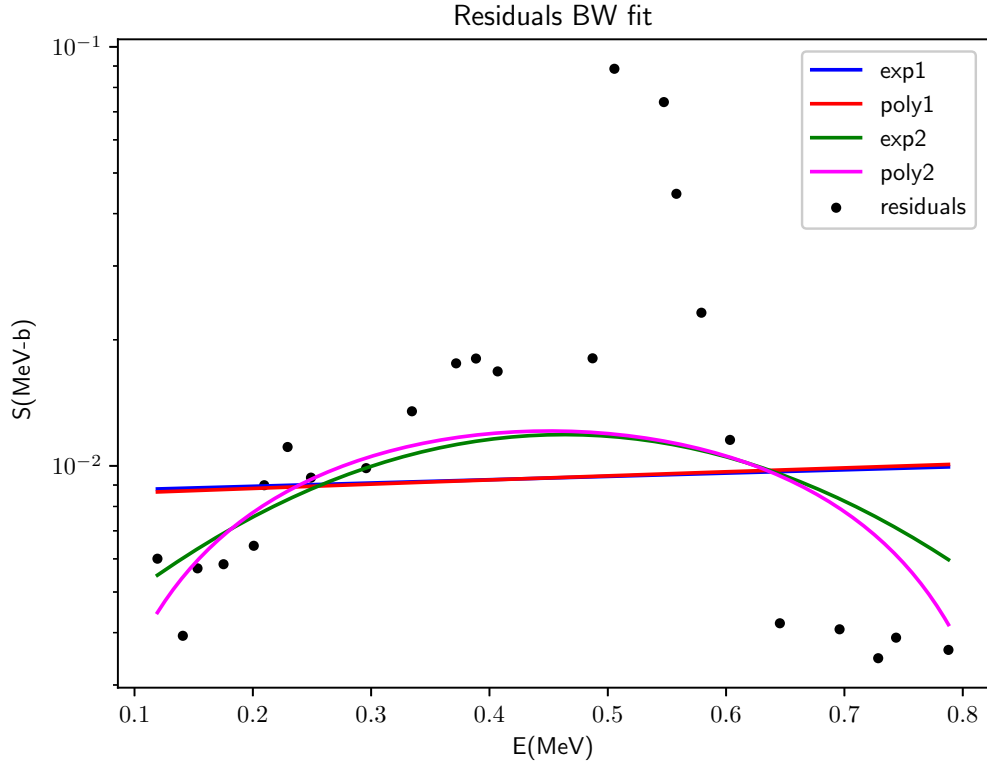
(c) Selected fits.

Figure 4.10: Empirical formulas fitted to background of the S-factor for the ^{13}C(p, γ)^{14}N reaction. The background was quantified with the residuals of the Breit-Wigner fit of Figure 4.9. he values of the fitting parameters are found in Tables C.11 and C.12.

The correspondence between the joint resonant and non-resonant prediction with experimental data at low energies improved at low energies. However, at energies above the resonance peak, the fit overestimated the S-factor.
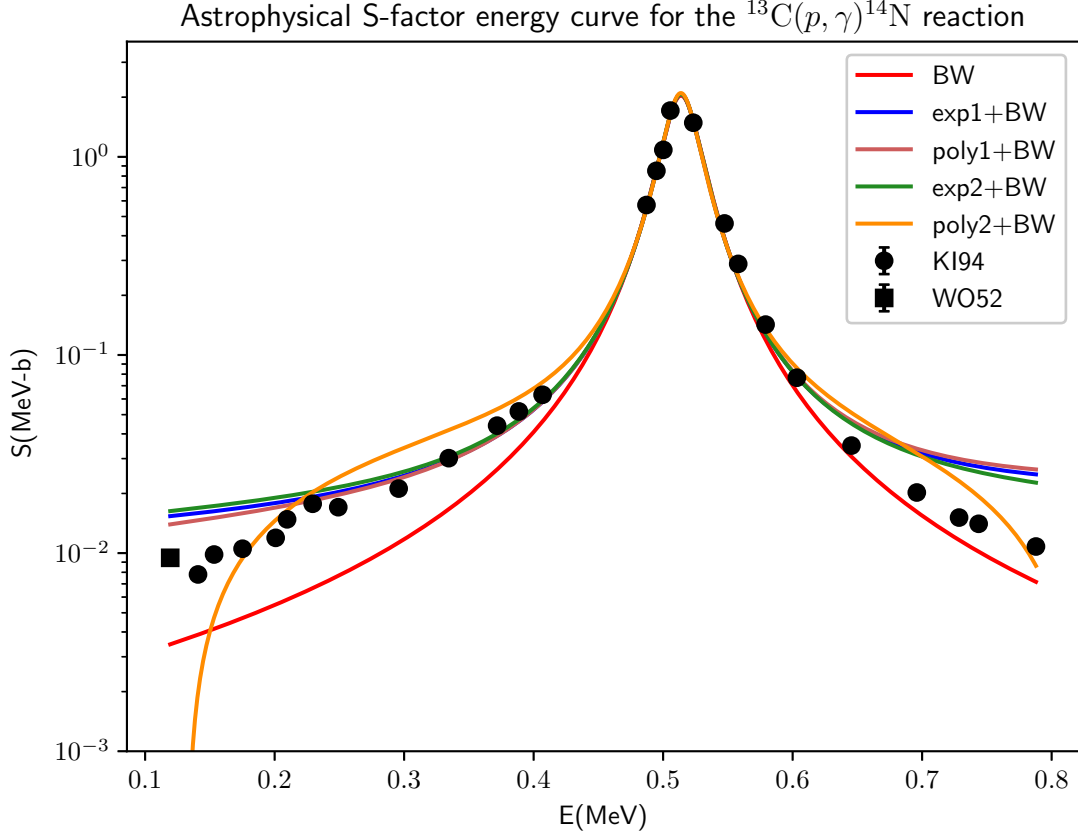
Figure 4.11: Empirical fit for the S-factor of the resonant ^{13}C(p, γ)^{14}N reaction. The resonant part was estimated with a Breit-Wigner fit added to a non-resonant background, which was fitted with exponential and polynomial with first and second order formulas. All the values of the parameters used are found in Table C.13.

This difference could be explained due to particularities of the physical phenomena underlying the ^{13}C(p, γ)^{14}N reaction. In fact, the S-factor values presented in Figure 4.9 corresponds to the sum of different channels associated with non-excited and excited states of ^{14}N [118]. This means that the theoretical prediction should consider the transitions to all possible states of the reactants and product nuclei.

The ^{12}C + ^{12}C channel have various resonances. These resonances could be explained from the Trojan Horse method or other alternative microscopical methods.

Chapter 5

Conclusions

Astrophysical S-factors were calculated for the selected reactions and compared with available experimental data.

Nuclear physics of stars. Christian Iliadis.

Cauldrons in the cosmos. Claus Rolfs.

Hyde and Basdevant Nuclear physics.

Appendix A

Literature selected data

A.1 General data of nuclei

In this section general data about the structure of the nuclei will be presented.
EXFOR [119].
Japanese database [120].

A.1.1 Selected constants

NIST selected constants and conversion factors to convenient units.

The units used for calculations are those suitable for calculations of astrophysical S-factors. In particular, the unit of energy is given in mega-electronvolts (MeV), and the distances between nuclei are given in fentometers (fm), and the cross sections in barns ($1b = 10^{-28}$cm). Therefore, various fundamental constant are converted to consistent units with respect to the mentioned convention as shown in the next table.

Some constants to be considered: c, h, $\hbar$, m_e, m_p, m_n.

In the units to be used for nuclear physics calculations: $4\pi\epsilon_0 = 1$. So, the fine structure constant is expressed as:

$$\alpha = \frac{e^2}{\hbar c}. \tag{A.1}$$

Therefore, the elementary charge is given by:

$$e = \sqrt{\alpha\hbar c} \approx \sqrt{1.41...}\sqrt{\text{MeV fm}}. \tag{A.2}$$

Masses can be expressed in terms of MeV/c^2 or MeV fm^{-2} s^2 depending on the context.

A.1.2 Nuclei structure data

atomic, massic, mass excess, spin, charge, data. L^π.

A.2 Astrophysical S-factor data

In this section, the reference to the experimental data on astrophysical S-factors for the selected reactions will be presented. In particular, the II database was widely used for reactions with $A < 10$. On the other hand, for reactions with $A > 10$, more specific references were used to obtain the experimental data.

Additional, light heavy experimental data pd reaction [121] and 2H proton capture c[122] and He3 photo-disintegration [123] with [124]

A.2.1 Nacre II database

The experimental data for a wide selection of radiative capture and exchange reactions at low energies is found in the Nacre II database [118]. This database serves as a compilation of data obtained form various experiments for the relevant reactions. In addition, in this paper a potential model calculation for each reaction is also included.

In the following tables, the references to the papers form which experimental data was obtained form this work will be presented.

Light nuclei reactions

Name	Reference	Reaction
GR85	[125]	
KR87a	[126]	
LE06a	[127]	^{2}H(d, p)^{3}H
RA02	[14]	
SC72	[128]	
TU11	[129]	
CA02	[130]	
FE65	[131]	
GE67	[132]	
GR62	[133]	^{2}H(p, γ)^{3}He
MA97	[134]	
SC96	[135]	
WA63	[124]	
WO67	[136]	

Table A.1: Experimental data references for a selection of non-resonant light heavy nuclei reactions. This table includes data corresponding to the ^{2}H(d, p)^{3}H and ^{2}H(p, γ)^{3}He reactions.

Resonant reactions

Name	Reference	Reaction
BA03	[137]	
JU03	[138]	^{7}Be(p, γ)^{8}B
JU10	[139]	
SC06	[140]	
KI94	[141]	^{13}C(p, γ)^{14}N
WO52	[142]	

Table A.2: Experimental data references for a selection of resonant reactions. This table includes data corresponding to the ^{7}Be(p, γ)^{8}B and ^{13}C(p, γ)^{14}N reactions.

A.2.2 Middle heavy nuclei data

Selected reaction reference table for the ^{12}C + ^{12}C, ^{12}C + ^{16}O, ^{16}O + ^{16}O , ^{13}C + ^{13}C reactions.
^{12}C + ^{12}C reaction.

Name	Reference	Reaction
Becker1981	[143]	$^{12}C + ^{12}C$
Fruet2020	[144]	
Spillane2007	[145]	
Tan2002	[146]	
Torilov21	[35]	$^{12}C + ^{16}O$
Thomas86	[32]	$^{16}O + ^{18}O$
		$^{16}O + ^{17}O$
Duarte2015	[30]	$^{16}O + ^{16}O$
Spinka1974	[147]	

Table A.3: Experimental data citations for a selection of oxygen and carbon fusion reactions.

A.2.3 Transitions data

Transition type data, energy levels.

A.3 Resonances and transitions

Resonant specific data will be presented. In particular, for those reactions with the aviable information, the experimental peak as well as the reaction peak will be detailed. Additionally, with special observance on the radiative capture reactions, the transitions will be specified.
Data on the resonant 7Be + p and experimental methods [148].

A.3.1 Resonance data

Selection reaction reference list.

A.3.2 Transitions data

Transition type data, energy levels, energy peak and widths.

A.4 Fitting parameters

The fitting parameters in a selected list of articles will be presented. In particular, this section distinguish between specific model parameters, like empirical, potential or microscopical models, and R-matrix fitting, whose special calculation considerations will be detailed.

A.4.1 Specific model parameters

Tables of models and parameters, with uncertainties.

A.4.2 R-matrix parameters

Tables of parameters that were chosen for the selected reactions

Appendix B

Special functions

In this section will be encountered special functions to be used in scattering theory and solution of analytical equations.

B.1   Bessel functions

Differential equation, solutions, 1st and 2nd kind and some useful properties. There are standard and spherical Bessel functions.

The spherical functions are solutions for the differential equation:

$$\frac{d^2 x}{d\rho^2} + 2\rho \frac{dx}{d\rho} + (\rho^2 - l(l+1))x = 0. \tag{B.1}$$

In particular, the solutions $J_l(\rho)$ and $Y_l(\rho)$ are called the Bessel and Von-Neumann solutions. One difference between these solutions is that $J_l(\rho)$ is well defined while $Y_l(\rho)$ has a pole at that $\rho = 0$.

In addition, the asymptotic behavior when $\rho \to \infty$ is different for each function as shown:

$$J_l(\rho) \to \sqrt{\frac{2}{\pi\rho}} \cos\left(\rho - \frac{\pi}{4} - \frac{l\pi}{2}\right). \tag{B.2}$$

and

$$Y_l(\rho) \to \sqrt{\frac{2}{\pi\rho}} \sin\left(\rho - \frac{\pi}{4} - \frac{l\pi}{2}\right). \tag{B.3}$$

B.2   Coulomb functions

Differential equations, solutions and more properties.

$$\frac{d^2 x}{d\rho^2} + (\rho^2 - 2\eta\rho - l(l+1))x = 0. \tag{B.4}$$

There are two solutions for this equations. In the context of scattering theory, the solutions $F_{l\eta}(\rho)$ and $G_{l\eta}(\rho)$ are analogous to the $J_l(\rho)$ and $Y_l(\rho)$ solutions of the Bessel differential equation respectively.

The formulas are connected as [149].

$$G_{l\eta} = \frac{F_{l\eta} - iF_{-l\eta}}{2i}. \tag{B.5}$$

In a similar way than the Bessel functions, the Coulomb functions have harmonic like asymptotic behavior. In particular, $F_{l\eta} \to \sin\theta_{l\eta}$ and $G_{l\eta} \to \cos\theta_{l\eta}$ with $\theta_{l\eta}$ defined as :

$$\theta_{l\eta}(\rho) = \rho - l\frac{\pi}{2} - \eta\ln(2\rho) + \arg\Gamma(l+1+i\eta). \tag{B.6}$$

B.3 Additional selected functions

Hypergeometric equations and connection with coulomb functions with implementation.

Spherical harmonics and Legendre polynomials for the expansions used in scattering theory. Hyperspherical harmonics

B.4 Clebsch-Gordan coefficients

Motivation, definition and some computations. Generalization to further spins and couplings that are useful for determining effects like the spin-orbit coupling.
The total angular momentum and change of basis.

$$J = L + S \tag{B.7}$$

.
Tensor products.

$$a \otimes b. \tag{B.8}$$

$$a \oplus b. \tag{B.9}$$

And the Wigner notation for the Clebsh-Gordan coefficients.

$$\begin{pmatrix} s & l & I_x \\ j_s & j & J \end{pmatrix}. \tag{B.10}$$

B.5 Microscopic model functions

Those relevant microscopic model methods. Specially, those that account for cluster model and effective field theory mod els.

Hamiltonians and Lagrangians of related field theories.

Appendix C

Fitting

This section is about fitting considerations on the different approaches used to calculate the astrophysical S-factor.

C.1 Empirical formulas fitting

Parameter list with uncertainty for its respective formula.

Polynomial. $^2\text{H}(\text{d}, \text{p})^3\text{H}$ reaction.

Label	g_0	g_1	g_2	g_3	g_4	g_5
poly1	0.0680 ± 0.0017	0.152 ± 0.0025				
poly2	0.0627 ± 0.0016	0.193 ± 0.0052	-0.0205 ± 0.0023			
poly3	0.0613 ± 0.0016	0.218 ± 0.011	-0.0523 ± 0.013	0.00847 ± 0.0034		
poly4	0.0615	0.212	-0.0401	0.00128	1.000	
poly5	0.0622 ± 0.0018	0.173 ± 0.032	0.116 ± 0.094	-0.189 ± 0.097	0.0886 ± 0.040	-0.0133 ± 0.0058
poly5-exclude	0.0554 ± 0.0013	0.254 ± 0.015	-0.0827 ± 0.041	-0.00712 ± 0.042	0.0197 ± 0.017	-0.00417 ± 0.0024

Table C.1: Fitting parameters of the polynomial fits, presented in Figures 4.1a and 4.1c, of the $^2\text{H}(\text{d}, \text{p})^3\text{H}$ reaction.

Exponential

Label	g_0	g_1	g_2	g_3	g_4	g_5
exp1	0.0929 ± 0.003	0.622 ± 0.019				
exp2	0.0724 ± 0.0018	1.397 ± 0.039	-0.271 ± 0.013			
exp3	0.066 ± 0.0016	2.028 ± 0.075	-0.888 ± 0.066	0.145 ± 0.015		
exp4	0.0674	1.847	-0.623	0.0191	1.000	
exp5	-2.789 ± 0.026	3.011 ± 0.22	-2.818 ± 0.51	1.495 ± 0.46	-0.384 ± 0.17	0.459 ± 0.023

Table C.2: Fitting parameters of the exponential fits, presented in Figure 4.1b, of the ^{2}H(d, p)^{3}H reaction.

Screening with poly5-exclude

Label	Comment	U_e(eV)
screening-all-fit	Fitting	100.0 ± 8.6
screening-only-RA02-fit	Fitting without RA02 data included	230.7 ± 9.2
screening-Ue-theory	Calculation with RA02 U_e value	309
RA02-paper	Prediction RA02 paper	

Table C.3: Screening effect parameter U_e values related to ^{2}H(d, p)^{3}H reaction fits presented in Figure 4.2. In the RA02-paper curve a poly1 for background estimation was used with parameters $g_0 = 0.0043$ and $g_1 = 0.54$ [14].

Polynomial.

Label	g_0	g_1	g_2	g_3	g_4	g_5
poly1-c	1.0 ± 1.5	10.00 ± 0.43				
poly2-c	1.0 ± 1.2	10.00 ± 0.93	0.309 ± 0.11			
poly3-c	0.0342 ± 1.1	10.0 ± 1.8	1.011 ± 0.55	-0.0839 ± 0.043		
poly4-c	0.253 ± 1.1	4.712 ± 3.30	4.803 ± 1.9	-0.830 ± 0.34	0.0432 ± 0.019	
poly5-c	0.434 ± 1.2	1.389 ± 5.96	7.980 ± 5.1	-1.829 ± 1.5	0.169 ± 0.19	-0.00547 ± 0.0081

Table C.4: Fitting parameters polynomial fits, shown in Figure 4.3a, ^{2}H(p, γ)^{3}He reaction.

Exponential

Label	g_0	g_1	g_2	g_3	g_4	g_5
exp1	12.958 ± 1.4	0.250 ± 0.014				
exp2	6.165 ± 0.86	0.649 ± 0.047	-0.0367 ± 0.038			
exp3	2.754 ± 0.64	1.334 ± 0.14	-0.181 ± 0.025	0.00865 ± 0.0014		
exp4	0.311 ± 0.45	2.116 ± 0.39	-0.447 ± 0.12	0.0439 ± 0.014	-0.00159 ± 0.00063	
exp5	0.315 ± 0.62	2.109 ± 0.73	-0.444 ± 0.33	0.0431 ± 0.067	-0.00151 ± 0.0064	-0.000294 ± 0.00023

Table C.5: Fitting parameters exponential fits, shown in Figure 4.3b, related to the ^{2}H(p, γ)^{3}He reaction.

Polynomial. ^{7}Be(p, γ)^{8}B reaction. Non-resonant background.

Label	g_0	g_1	g_2	g_3	g_4	g_5	g_6
poly1	18.429 ± 0.86	7.668 ± 1.1					
poly2	18.316 ± 1.3	8.042 ± 3.3	-0.217 ± 1.8				
poly3	13.868 ± 2.3	29.490 ± 10.0	-24.403 ± 10.8	7.101 ± 3.1			
poly4	15.075	22.690	-13.835	1.106	0.000		
poly5	13.219 ± 5.4	27.594 ± 35.8	-0.187 ± 79.8	-35.841 ± 78.3	26.055 ± 34.3	-5.072 ± 5.4	
poly6	27.181 ± 7.7	-103.057 ± 63.1	419.070 ± 185.7	-631.656 ± 251.3	435.745 ± 167.9	-138.269 ± 53.8	16.382 ± 6.6

Table C.6: Parameters polynomial fits, included in Figure 4.7a, corresponding to ^{7}Be(p, γ)^{8}B reaction.

Exponential

Label	g_0	g_1	g_2	g_3	g_4	g_5	g_6
exp1	19.091 ± 0.71	0.301 ± 0.042					
exp2	18.731 ± 1.1	0.356 ± 0.13	-0.0278 ± 0.060				
exp3	16.162 ± 1.5	1.024 ± 0.36	-0.734 ± 0.36	0.194 ± 0.096			
exp4	16.985	0.770	-0.388	0.0261	0.000		
exp5	2.645 ± 0.29	1.355 ± 1.9	0.295 ± 4.3	-2.425 ± 4.2	1.720 ± 1.9	-0.344 ± 0.30	
exp6	3.071 ± 0.36	-2.499 ± 2.7	12.451 ± 7.5	-19.720 ± 9.6	13.799 ± 6.1	-4.382 ± 1.9	0.516 ± 0.22

Table C.7: Parameters exponential fits, included in Figure 4.7b, associated with the ^{7}Be(p, γ)^{8}B reaction.

BW ^{7}Be(p, γ)^{8}B

Label	S_r(MeV b)	E_r(MeV)	Γ_r(MeV)
BW	99.153 $\pm$ 4.9	0.632 $\pm$ 0.0010	0.0535 $\pm$ 0.0034

Table C.8: Fitting parameters to the Breit-Wigner function, shown in Figure 4.7c, for the ^{7}Be(p, γ)^{8}B reaction.

Composite ^{7}Be(p, γ)^{8}B

Label	S_r(MeV b)	E_r(MeV)	Γ_r(MeV)	c_r(MeV^2)	g_0	g_1
exp + BW	87.097 $\pm$ 2.2	0.631 $\pm$ 0.00036	0.0335 $\pm$ 0.00095		17.935 $\pm$ 0.13	0.325 $\pm$ 0.0077
poly + BW	21.227	0.631 $\pm$ 0.00062	0.0331	0.00113	17.370 $\pm$ 0.20	7.725 $\pm$ 0.27

Table C.9: Fitting parameters for composite resonant and non-resonant behavior fits, as visualized in Figure 4.8, for the ^{7}Be(p, γ)^{8}B reaction.

BW ^{13}C(p, γ)^{14}N

Label	S_r(MeV b)	E_r(MeV)	Γ_r(MeV)
BW	2.040 $\pm$ 0.059	0.514 $\pm$ 0.00026	0.0325 $\pm$ 0.0013

Table C.10: Fitting parameters Breit-Wigner fits, included in Figure 4.9, related to the ^{13}C(p, γ)^{14}N reaction.

Residuals polynomial fit ^{13}C(p, γ)^{14}N reaction.

Label	g_0	g_1	g_2	g_3	g_4
poly1	0.00841 $\pm$ 0.016	0.00211 $\pm$ 0.033			
poly2	-0.00204 $\pm$ 0.032	0.0628 $\pm$ 0.17	-0.0697 $\pm$ 0.19		
poly3	0.00694 $\pm$ 0.076	-0.0193 $\pm$ 0.65	0.135 $\pm$ 1.6	-0.150 $\pm$ 1.1	
poly4	0.00678	-0.0134	0.0943	-0.0606	1.000

Table C.11: Fitting parameters polynomial fit residuals, as visible in Figure 4.10a, for the ^{13}C(p, γ)^{14}N reaction.

Residuals exponential fit ^{13}C(p, γ)^{14}N reaction.

Label	g_0	g_1	g_2	g_3	g_4
exp1	0.00862 $\pm$ 0.015	0.181 $\pm$ 3.6			
exp2	0.00292 $\pm$ 0.013	6.049 $\pm$ 21.3	-6.526 $\pm$ 23.9		
exp3	0.0238 $\pm$ 0.23	-13.564 $\pm$ 83.3	42.626 $\pm$ 205.1	-36.166 $\pm$ 153.3	
exp4	0.0306	-15.084	39.610	-17.343	0.000

Table C.12: Fitting parameters exponential fit t residuals, as shown in Figure 4.10b, for the ^{13}C(p,γ)^{14}N reaction.

Composite ^{13}C(p,γ)^{14}N

Label	S_r	E_r	Γ_r	c_r	g_0	g_1	g_2
exp1 + BW	2.056 $\pm$ 0.062	0.514 $\pm$ 0.00025	0.0314 $\pm$ 0.0014		0.0113 $\pm$ 0.014	0.612 $\pm$ 2.4	
poly1 + BW	2.057	0.514 $\pm$ 0.00026	0.0314	0.000247 $\pm$ 0.0014	0.00910 $\pm$ 0.017	0.0135 $\pm$ 0.037	
exp2 + BW	2.057 $\pm$ 0.063	0.514 $\pm$ 0.00026	0.0314 $\pm$ 0.0015		0.0117 $\pm$ 0.033	1.0 $\pm$ 15.1	-0.770 $\pm$ 16.3
poly2 + BW	2.041	0.514 $\pm$ 0.00025	0.031 $\pm$ 0.0015	0.000236	-0.037 $\pm$ 0.039	0.294 $\pm$ 0.22	-0.310 $\pm$ 0.24

Table C.13: Fitting parameters composite fits, included in Figure 4.11, corresponding to the ^{13}C(p,γ)^{14}N reaction.

C.2 Free parameters fitting on potential models

Parameter list, uncertainty and its respective formula.
[150] Sao Pablo potential.

[151] Woods-Saxon potential.

C.3 Microscopic model fitting

Parameter list, uncertainty and its respective formula.
[152]

C.4 R-matrix fitting

Parameter list, uncertainty and its respective formula. Widths and channels.

Reaction	E_R(MeV)	Γ(MeV)	References
1	0.504	0.102	REF1
4	0.607	0.304	REF2

Table C.14: A new Table

[153] [154] [155]

Appendix D

Numerical integration and differential equation solving

In this section will be introduced the generalities of the numerical solution of integrals and differential equation that were used throughout the document. In particular, a special subsection on the numerical solution for the Schroödinger equation for scattering phenomena will be presented.

D.1   Integration of selected potentials

WKB numerical implementation based on the Gaussian quadrature algorithm.

D.2   Numerical solution of the Schrödinger equation

The numerical solution of the Schrödinger equation is found to be useful for the approaches where it is not possible to find a solution for the problem in closed form, mainly analytical solutions.
[156]
Coupled channels [157].

D.2.1   Main approach

The different methods to be solved the Schroödinger equation and overall differential equation solving strategy.

D.2.2   Implementation of the potential functions

Different potential considerations.

D.2.3   Boundary conditions implementation

Expected boundary conditions at $r \to \infty$ and their numerical implementation.

Appendix E

Computer codes implementation

In this section is going to be presented the aspects related with the `sfactors` python module.

E.1   Structure of the computer program

The full tree with the files with explanation of the detailed packages.

E.2   User manual

In this section the user manual should be presented.

E.2.1   Installation

In this section a full installation sequence will be presented

E.2.2   Plotting

Plotting of S-factors.

E.2.3   Empirical fitting

Empirical fitting based on predetermined and custom functions.

E.2.4   Specific model fitting

Model fitting.

E.2.5   Model testing

Different tests of the program code.

E.3   Documentation

E.3.1   Databases

E.3.2   Non resonant

Bibliography

[1] J. L. Basdevant, J. Rich, and M. Spiro. *Fundamentals in nuclear physics: From nuclear structure to cosmology.* Springer Verlag New York, 2004.

[2] K. Heyde. *Basic ideas and concepts in nuclear physics: An introductory approach.* CRC Press, 2020.

[3] C. Iliadis. *Nuclear physics of stars.* Wiley-VCH, 2015.

[4] R. Dick. *Advanced Quantum Mechanics: Materials and photons.* Springer, 2016.

[5] C. J. Joachain. *Quantum collision theory.* North-Holland Pub. Co., 1983.

[6] R. G. Newton. *Quantum Physics: A Text for Graduate Students.* Graduate Texts in Contemporary Physics. Springer, 2002.

[7] H. Sasaki, T. Kawano, and I. Stetcu. Noniterative finite amplitude methods for $E1$ and $M1$ giant resonances. *Physical Review C*, 105(4), 2022.

[8] C. A. Bertulani. Nuclear reactions. *digital Encyclopedia of Applied Physics*, page 45–92, 2003.

[9] C. R. Brune and B. Davids. Radiative capture reactions in astrophysics. *Annual Review of Nuclear and Particle Science*, 65(1):87–112, 2015.

[10] T. R. Whitehead, T. Poxon-Pearson, F. M. Nunes, and G. Potel. Prediction for (p, n) charge-exchange reactions with uncertainty quantification. *Physical Review C*, 105(5), 2022.

[11] A. Sharma, A. Gandhi, and A. Kumar. Investigation of Weisskopf-Ewing approximation for the determination of (n, p) cross sections using the surrogate reaction technique. *Physical Review C*, 105(1), 2022.

[12] C. A. Bertulani and T. Kajino. Frontiers in nuclear astrophysics. *Progress in Particle and Nuclear Physics*, 89:56–100, 2016.

[13] P. Descouvemont. Nuclear reactions of astrophysical interest. *Frontiers in Astronomy and Space Sciences*, 7, 2020.

[14] F. Raiola, P. Migliardi, G. Gyürky, M. Aliotta, A. Formicola, R. Bonetti, C. Broggini, L. Campajola, P. Corvisiero, H. Costantini, and et al. Enhanced electron screening in d(d,p)t for deuterated Ta*. *The European Physical Journal A*, 13(3):377–382, 2002.

[15] H. J. Assenbaum, K. Langanke, and C. Rolfs. Effects of electron screening on low-energy fusion cross sections. *Zeitschrift für Physik A Atomic Nuclei*, 327(4):461–468, 1987.

[16] E. Margaret Burbidge, G. R. Burbidge, W. A. Fowler, and F. Hoyle. Synthesis of the Elements in Stars. *Reviews of Modern Physics*, 29(4):547–650, 1957.

[17] G. Lotay, D. T. Doherty, R. V. Janssens, D. Seweryniak, H. M. Albers, S. Almaraz-Calderon, M. P. Carpenter, A. E. Champagne, C. J. Chiara, C. R. Hoffman, and et al. Revised decay properties of the key 93-keV resonance in the ^{25}Mg(p, γ) reaction and its influence on the MgAl cycle in astrophysical environments. *Physical Review C*, 105(4), 2022.

[18] C. Spitaleri, A. M. Mukhamedzhanov, L. D. Blokhintsev, M. La Cognata, R. G. Pizzone, and A. Tumino. The Trojan Horse Method in Nuclear Astrophysics. *Physics of Atomic Nuclei*, 74(12):1725–1739, 2011.

[19] M. Pignatari, R. Hirschi, M. Wiescher, R. Gallino, M. Bennett, M. Beard, C. Fryer, F. Herwig, G. Rockefeller, F. X. Timmes, and et al. The ^{12}C + ^{12}C reaction and the impact on nucleosynthesis in massive stars. *The Astrophysical Journal*, 762(1):31, 2012.

[20] A. Diaz-Torres and M. Wiescher. Characterizing the astrophysical S factor for ^{12}C + ^{12}C fusion with wave-packet dynamics. *Physical Review C*, 97(5), 2018.

[21] Y. J. Li, X. Fang, B. Bucher, K. A. Li, L. H. Ru, and X. D. Tang. Modified astrophysical S-factor of ^{12}C + ^{12}C fusion reaction at sub-barrier energies. *Chinese Physics C*, 44(11):115001, 2020.

[22] T.-P. Luo, P.-W. Wen, C.-J. Lin, L. Yang, H.-M. Jia, F. Yang, D.-H. Huang, C. Chang, M.-H. Zhang, Y. Yang, and et al. Bayesian analysis on non-resonant behavior of ^{12}C + ^{12}C fusion reaction at sub-barrier energies. *Chinese Physics C*, 46(6):064105, 2022.

[23] A. M. Mukhamedzhanov, D. Y. Pang, and A. S. Kadyrov. Astrophysical factors of ^{12}C + ^{12}C fusion extracted using the Trojan horse method. *Physical Review C*, 99(6), 2019.

[24] A. M. Mukhamedzanov. Status of deep subbarrier ^{12}C + ^{12}C fusion and advancing the Trojan horse method. *The European Physical Journal A*, 58(4), 2022.

[25] Y. Taniguchi and M. Kimura. ^{12}C + ^{12}C fusion S^*-factor from a full-microscopic nuclear model. *Physics Letters B*, 823:136790, 2021.

[26] M. Assunção and P. Descouvemont. ^{12}C + ^{12}C fusion in a multichannel folding model. *Journal of Physics: Conference Series*, 665:012010, 2016.

[27] F. Koyuncu and A. Soylu. Screening effects on ^{12}C + ^{12}C fusion reaction. *Chinese Physics C*, 42(5):054106, 2018.

[28] M. Notani, H. Esbensen, X. Fang, B. Bucher, P. Davies, C. L. Jiang, L. Lamm, C. J. Lin, C. Ma, E. Martin, and et al. Correlation between the ^{12}C + ^{12}C, ^{12}C + ^{13}C, and ^{13}C + ^{13}C fusion cross sections. *Physical Review C*, 85(1), 2012.

[29] N. T. Zhang, X. Y. Wang, D. Tudor, B. Bucher, I. Burducea, H. Chen, Z. J. Chen, D. Chesneanu, A. I. Chilug, L. R. Gasques, and et al. Constraining the ^{12}C + ^{12}C astrophysical S-factors with the ^{12}C + ^{13}C measurements at very low energies. *Physics Letters B*, 801:135170, 2020.

[30] J. G. Duarte, L. R. Gasques, J. R. Oliveira, V. A. Zagatto, L. C. Chamon, N. H. Medina, N. Added, W. A. Seale, J. A. Alcántara-Núñez, E. S. Rossi, and et al. Measurement of fusion cross sections for ^{16}O + ^{16}O. *Journal of Physics G: Nuclear and Particle Physics*, 42(6):065102, 2015.

[31] A. Kuronen, J. Keinonen, and P. Tikkanen. Cross section of ^{16}O + ^{16}O near the Coulomb barrier. *Physical Review C*, 35(2):591–596, 1987.

[32] J. Thomas, Y. T. Chen, S. Hinds, D. Meredith, and M. Olson. Sub-barrier fusion of the oxygen isotopes: A more complete picture. *Physical Review C*, 33(5):1679–1689, 1986.

[33] L. Guimin, F. Deji, and C. Xiaowu. Sub-Barrier Fusion Coupled-Channels Calculations for ^{16}O + ^{16,18}O. *Chinese Physics Letters*, 9(11):577–580, 1992.

[34] J. L. Ferreira, J. Lubian, R. Linares, M. J. Ermamatov, H. Yépez-Martínez, and P. O. Hess. Analysis of the alpha-transfer reaction in the ^{12}C + ^{16}O system using the semi-microscopic algebraic cluster model. *The European Physical Journal A*, 55(6), 2019.

[35] S. Y. Torilov, N. A. Maltsev, and V. I. Zherebchevsky. Studying Low-Energy Resonances in the ^{12}C + ^{16}O system. *Bulletin of the Russian Academy of Sciences: Physics*, 85(5):548–551, 2021.

[36] Y.-D. Chan, H. Bohn, R. Vandenbosch, R. Sielemann, J. G. Cramer, K. G. Bernhardt, H. C. Bhang, and D. T. Chiang. Influence of Extra Neutrons Added to the ^{12}C + ^{16}O System: Gross Structures in γ-ray Yields Following the ^{13}C + ^{16}O and ^{12}C + ^{18}O reactions. *Physical Review Letters*, 42(11):687–690, 1979.

[37] D. G. Kovar, D. F. Geesaman, T. H. Braid, Y. Eisen, W. Henning, T. R. Ophel, M. Paul, K. E. Rehm, S. J. Sanders, P. Sperr, and et al. Systematics of carbon- and oxygen-induced fusion on nuclei with $12 \leq A \leq 19$. *Physical Review C*, 20(4):1305–1331, 1979.

[38] B. Wang, Z. Ren, and D. Bai. $^{16-18}$O + ^{16}O and ^{16,18}O + ^{12,13}C fusion-evaporation reactions at near-Coulomb-barrier energies from statistical model calculations. *Physical Review C*, 101(2), 2020.

[39] M. Assunção and P. Descouvemont. ^{12}C + ^{12}C and ^{16}O + ^{16}O fusion reactions at low energies. *Journal of Physics: Conference Series*, 590:012038, 2015.

[40] P. Descouvemont. Resonances in ^{12}C and ^{24}Mg: what do we learn from a microscopic cluster theory? *The European Physical Journal A*, 57(1), 2021.

[41] G. Montagnoli, A. M. Stefanini, C. L. Jiang, G. Colucci, A. Goasduff, D. Brugnara, M. Mazzocco, M. Siciliano, F. Scarlassara, L. Corradi, and et al. Study of fusion hindrance in the system ^{12}C + ^{24}Mg. *Journal of Physics: Conference Series*, 1643(1):012098, 2020.

[42] G. P. Nobre, L. C. Chamon, L. R. Gasques, B. V. Carlson, and I. J. Thompson. Consistent analysis of fusion data without adjustable parameters for a wide variety of heavy-ion systems. *Physical Review C*, 75(4), 2007.

[43] A. Arcones, D. W. Bardayan, T. C. Beers, L. A. Bernstein, J. C. Blackmon, B. Messer, B. A. Brown, E. F. Brown, C. R. Brune, A. E. Champagne, and et al. White paper on nuclear astrophysics and low energy nuclear physics Part 1: Nuclear astrophysics. *Progress in Particle and Nuclear Physics*, 94:1–67, 2017.

[44] J. Carlson, M. P. Carpenter, R. Casten, C. Elster, P. Fallon, A. Gade, C. Gross, G. Hagen, A. C. Hayes, D. W. Higinbotham, and et al. White paper on nuclear astrophysics and low-energy nuclear physics, Part 2: Low-energy nuclear physics. *Progress in Particle and Nuclear Physics*, 94:68–124, 2017.

[45] B. R. Barrett, P. Navrátil, and J. P. Vary. *Ab Initio* no core shell model. *Progress in Particle and Nuclear Physics*, 69:131–181, 2013.

[46] C. Beck. *Clusters in nuclei, vol. 2.* Springer Berlin Heidelberg, 2012.

[47] L. E. Marcucci, K. M. Nollett, R. Schiavilla, and R. B. Wiringa. Modern theories of low-energy astrophysical reactions. *Nuclear Physics A*, 777:111–136, 2006.

[48] L. V. Grigorenko, B. V. Danilin, V. D. Efros, N. B. Shul'gina, and M. V. Zhukov. Structure of the ^{8}Li and ^{8}B nuclei in an extended three-body model and astrophysical S_{17} factor. *Physical Review C*, 57(5), 1998.

[49] T. Neff, H. Feldmeier, and K. Langanke. Towards microscopic ab initio calculations of astrophysical S-factors. *Progress in Particle and Nuclear Physics*, 66(2):341–345, 2011.

[50] P. Navrátil, S. Quaglioni, G. Hupin, C. Romero-Redondo, and A. Calci. Unified *ab initio* approaches to nuclear structure and reactions. *Physica Scripta*, 91(5):053002, 2016.

[51] P. Navratil, C. A. Bertulani, and E. Caurier. ^{7}Be(p, γ)^{8}B S-factor from ab *initio* wave functions. *Journal of Physics: Conference Series*, 49:15–20, 2006.

[52] M. C. Atkinson, P. Navrátil, G. Hupin, K. Kravvaris, and S. Quaglioni. *Ab initio* calculation of the β decay from ^{11}Be to a ^{10}Be + p resonance. *Physical Review C*, 105(5), 2022.

[53] K. Arai, S. Aoyama, Y. Suzuki, P. Descouvemont, and D. Baye. Tensor force manifestations in *ab initio* study of the ^{2}H(d, γ)^{4}He, ^{2}H(d, p)^{3}H and ^{2}H(d, n)^{3}He reactions. *Journal of Physics: Conference Series*, 436:012024, 2013.

[54] J. Dohet-Eraly, P. Navrátil, S. Quaglioni, W. Horiuchi, G. Hupin, and F. Raimondi. ^{3}He(α, γ)^{7}Be and ^{3}H(α, γ)^{7}Li astrophysical S factors from the no-core shell model with continuum. *Physics Letters B*, 757:430–436, 2016.

[55] G. X. Dong, X. B. Wang, N. Michel, and M. Płoszajczak. Gamow shell model description of the radiative capture reaction ^{8}Li(n, γ)^{9}Li. *Physical Review C*, 105(6), 2022.

[56] T. Tazawa. Nucleus-Nucleus potential in the Two-Center Shell Model. *Progress of Theoretical Physics*, 51(6):1764–1782, 1974.

[57] H. Sadeghi, H. Khalili, and M. Godarzi. Astrophysical S-factor of the d(p, γ)^{3}He process by effective field theory. *Chinese Physics C*, 37(4):044102, 2013.

[58] R. Higa, P. Premarathna, and G. Rupak. Coupled-channels treatment of ^{7}Be(p, γ)^{8}B in effective field theory. *Physical Review C*, 106(1), 2022.

[59] M. Dufour and P. Descouvemont. Multicluster study of the ^{12}C + n and ^{12}C + p systems. *Physical Review C*, 56(4):1831–1839, 1997.

[60] C. Simenel, R. Keser, A. S. Umar, and V. E. Oberacker. Microscopic study of ^{16}O + ^{16}O fusion. *Physical Review C*, 88(2), 2013.

[61] H. Jayatissa, M. L. Avila, K. E. Rehm, R. Talwar, P. Mohr, K. Auranen, J. Chen, D. A. Gorelov, C. R. Hoffman, C. L. Jiang, and et al. First direct measurement of the ^{13}N(α, p)^{16}O reaction relevant for core-collapse supernovae nucleosynthesis. *Physical Review C*, 105(4), 2022.

[62] Shubhchintak and P. Descouvemont. Breakup effects in the ^{16}C + p and ^{16}C + d reactions. *Physical Review C*, 105(2), 2022.

[63] T. Baba, Y. Taniguchi, and M. Kimura. 4α linear-chain state produced by ^{9}Be + ^{9}Be collisions. *Physical Review C*, 105(6), 2022.

[64] N. Le Anh and B. Minh Loc. Low-energy ^{7}Li(n, γ)^{8}Li and ^{7}Be(p, γ)^{8}B radiative capture reactions within the Skyrme Hartree-Fock approach. *Physical Review C*, 106(1), 2022.

[65] A. M. Lane and R. G. Thomas. R-matrix theory of nuclear reactions. *Reviews of Modern Physics*, 30(2):257–353, 1958.

[66] P. Descouvemont and D. Baye. The *R*-matrix theory. *Reports on Progress in Physics*, 73(3):036301, 2010.

[67] D. F. Ramírez Jiménez and N. G. Kelkar. Different manifestations of S-matrix poles. *Annals of Physics*, 396:18–43, 2018.

[68] R. S. de Souza, C. Iliadis, and A. Coc. Astrophysical S-factors, Thermonuclear Rates, and Electron Screening Potential for the ${}^3\mathrm{He}(\mathrm{d}, \mathrm{p}){}^4\mathrm{He}$ Big Bang Reaction via a Hierarchical Bayesian Model. *The Astrophysical Journal*, 872(1):75, 2019.

[69] R. Spartá, R. G. Pizzone, C. A. Bertulani, S. Hou, L. Lamia, and A. Tumino. Direct and Indirect Measurements for a Better Understanding of the Primordial Nucleosynthesis. *Frontiers in Astronomy and Space Sciences*, 7, 2020.

[70] D. Odell, C. R. Brune, and D. R. Phillips. How bayesian methods can improve R-matrix analyses of data: The example of the *dt* reaction. *Physical Review C*, 105(1), 2022.

[71] J. Grineviciute, L. Lamia, A. M. Mukhamedzhanov, C. Spitaleri, and M. La Cognata. Low-energy R-matrix fits for the ${}^6\mathrm{Li}(\mathrm{d}, \alpha){}^4\mathrm{He}$ S factor. *Physical Review C*, 91(1), 2015.

[72] B. Vande Kolk, K. T. Macon, R. J. deBoer, T. Anderson, A. Boeltzig, K. Brandenburg, C. R. Brune, Y. Chen, A. M. Clark, T. Danley, and et al. Investigation of the ${}^{10}\mathrm{B}(\mathrm{p}, \alpha){}^7\mathrm{Be}$ reaction from 0.8 to 2.0 MeV. *Physical Review C*, 105(5), 2022.

[73] A. Sieverding, J. S. Randhawa, D. Zetterberg, R. J. deBoer, T. Ahn, R. Mancino, G. Martínez-Pinedo, and W. R. Hix. Role of low-lying resonances for the ${}^{10}\mathrm{Be}(\mathrm{p}, \alpha){}^7\mathrm{Li}$ reaction rate and implications for the formation of the Solar System. *Physical Review C*, 106(1), 2022.

[74] G. Kaur, V. Guimarães, J. C. Zamora, M. Assunção, J. Alcantara-Nuñez, A. L. de Lara, E. O. Zevallos, J. B. Ribeiro, R. Lichtenthäler, K. C. Pires, and et al. New resonances in ${}^{11}\mathrm{C}$ above the ${}^{10}\mathrm{B}+p$ threshold investigated by inverse kinematic resonant scattering. *Physical Review C*, 105(2), 2022.

[75] D. Schürmann, L. Gialanella, R. Kunz, and F. Strieder. The astrophysical S factor of ${}^{12}\mathrm{C}(\alpha, \gamma){}^{16}\mathrm{O}$ at stellar energy. *Physics Letters B*, 711(1):35–40, 2012.

[76] J.-M. Sparenberg. Hybrid potential/R-matrix models for the $12\mathrm{C} + \alpha$ system. *Nuclear Physics A*, 758:423–426, 2005.

[77] P. S. Prusachenko, T. L. Bobrovsky, I. P. Bondarenko, M. V. Bokhovko, A. F. Gurbich, and V. V. Ketlerov. Measurement of the cross section for the ${}^{13}\mathrm{C}(\alpha, \mathrm{n}){}^{16}\mathrm{O}$ reaction and determination of the cross section for the ${}^{16}\mathrm{O}(\mathrm{n}, \alpha){}^{13}\mathrm{C}$ reaction. *Physical Review C*, 105(2), 2022.

[78] N. Burtebaev, S. B. Igamov, R. J. Peterson, R. Yarmukhamedov, and D. M. Zazulin. New measurements of the astrophysical S factor for ${}^{12}\mathrm{C}(\mathrm{p}, \gamma){}^{13}\mathrm{N}$ reaction at low energies and the asymptotic normalization coefficient (nuclear vertex constant) for the $p + {}^{12}\mathrm{C} \rightarrow {}^{13}\mathrm{N}$ reaction. *Physical Review C*, 78(3), 2008.

[79] S. Chakraborty, R. deBoer, A. Mukherjee, and S. Roy. Systematic R-matrix analysis of the ${}^{13}\mathrm{C}(\mathrm{p}, \gamma){}^{14}\mathrm{N}$ capture reaction. *Physical Review C*, 91(4), 2015.

[80] G. Genard, P. Descouvemont, and G. Terwagne. S-factor measurement of the ${}^{13}\mathrm{C}(\mathrm{p}, \gamma){}^{14}\mathrm{N}$ reaction in reverse kinematics. *Journal of Physics: Conference Series*, 202:012015, 2010.

[81] F. C. Barker. ${}^{15}\mathrm{N}(\mathrm{p}, \gamma_0){}^{16}\mathrm{O}$ S factor. *Physical Review C*, 78(4), 2008.

[82] C. Angulo, A. E. Champagne, and H.-P. Trautvetter. R-matrix analysis of the ${}^{14}\mathrm{N}(\mathrm{p}, \gamma){}^{15}\mathrm{O}$ astrophysical S-factor. *Nuclear Physics A*, 758:391–394, 2005.

[83] A. Formicola, G. Imbriani, H. Costantini, C. Angulo, D. Bemmerer, R. Bonetti, C. Broggini, P. Corvisiero, J. Cruz, P. Descouvemont, and et al. Astrophysical S-factor of ${}^{14}\mathrm{N}(\mathrm{p}, \gamma){}^{15}\mathrm{O}$. *Physics Letters B*, 591(1-2):61–68, 2004.

[84] J. Humblet. K-matrix analysis of resonance nuclear reactions. *Physical Review C*, 42(4):1582–1591, 1990.

[85] C. R. Brune. Alternative parametrization of *R*-matrix theory. *Physical Review C*, 66(4), 2002.

[86] D. G. Yakovlev, M. Beard, L. R. Gasques, and M. Wiescher. Simple analytic model for astrophysical *S* factors. *Physical Review C*, 82(4), 2010.

[87] R. Ghasemi and H. Sadeghi. S-factor for radiative capture reactions for light nuclei at astrophysical energies. *Results in Physics*, 9:151–165, 2018.

[88] S. Dubovichenko and A. Dzhazairov-Kakhramanov. Examination of the astrophysical S-factors of the radiative proton capture on ^{2}H, ^{6}Li, ^{7}Li, ^{12}C and ^{13}C. *International Journal of Modern Physics E*, 21(03):1250039, 2012.

[89] E. M. Tursunov, S. A. Turakulov, A. S. Kadyrov, and L. D. Blokhintsev. Astrophysical S factor and rate of ^{7}Be(p, γ)^{8}B direct capture reaction in a potential model. *Physical Review C*, 104(4), 2021.

[90] C. A. Bertulani. ^{7}Be(p, γ)^{8}B cross section from indirect breakup experiments. *Zeitschrift für Physik A: Hadrons and Nuclei*, 356(1):293–297, 1996.

[91] A. Kabir and J.-U. Nabi. Re-examination of astrophysical S-factor of proton capture ^{9}Be(p, γ)^{10}B in stellar matter. *Nuclear Physics A*, 1007:122118, 2021.

[92] S. B. Dubovichenko and A. V. Dzhazairov-Kakhramanov. Astrophysical S -factor of p^{2}H radiative capture. *The European Physical Journal A*, 39(2):139–143, 2009.

[93] K. Czerski, A. Huke, P. Heide, and G. Ruprecht. Experimental and theoretical screening energies for the ^{2}H(d, p)^{3}H reaction in metallic environments. *The European Physical Journal A*, 27(S1):83–88, 2006.

[94] A. Kabir, B. F. Irgaziev, and J.-U. Nabi. Radiative capture of proton by ^{13}C at low energy. *Astrophysics and Space Science*, 365(6), 2020.

[95] S. B. Dubovichenko. Astrophysical *S*-factor for the radiative-capture reaction p^{13}C → ^{14}Nγ. *Physics of Atomic Nuclei*, 75(2):173–181, 2012.

[96] A. Kabir, B. F. Irgaziev, J.-U. Nabi, and S. Sagheer. Re-analysis of radiative capture ^{11}C(p, γ)^{12}N at low energy. *Journal of Physics G: Nuclear and Particle Physics*, 49(7):075101, 2022.

[97] A. Diaz-Torres, L. R. Gasques, and M. Wiescher. Effects of nuclear molecular configurations on the astrophysical S-factor for ^{16}O + ^{16}O. *Physics Letters B*, 652(5-6):255–258, 2007.

[98] L. C. Chamon. The São Paulo potential. *Nuclear Physics A*, 787(1-4):198–205, 2007.

[99] A. H. Amer and Y. E. Penionzhkevich. Elastic scattering analysis of isobar nuclei $A = 6$ projectiles on ^{12}C using different models of optical potential. *Nuclear Physics A*, 1015:122300, 2021.

[100] P. Salamon, Á. Baran, and T. Vertse. Distributions of the S-matrix Poles in Woods–Saxon and cut-off Woods–Saxon potentials. *Nuclear Physics A*, 952:1–17, 2016.

[101] M. Singh, Sukhvinder, and R. Kharab. Analysis of fusion excitation functions of various systems using modified Woods–Saxon potential. *Nuclear Physics A*, 897:179–197, 2013.

[102] M. Singh, Sukhvinder, and R. Kharab. Analysis of fusion excitation function data by using an energy dependent potential model. *Nuclear Physics A*, 897:198–217, 2013.

[103] R. Bass. Nucleus-Nucleus Potential Deduced from Experimental Fusion Cross Sections. *Physical Review Letters*, 39(5):265–268, 1977.

[104] T. Nandi, D. K. Swami, P. S. Gupta, Y. Kumar, S. Chakraborty, and H. C. Manjunatha. Search for a viable nucleus–nucleus potential in heavy-ion nuclear reactions. *Pramana*, 96(2), 2022.

[105] B. K. Jennings, S. Karataglidis, and T. D. Shoppa. Direct capture astrophysical S factors at low energy. *Physical Review C*, 58(1):579–581, 1998.

[106] M. I. Hussein and R. H. Abdullah. Calculation of astrophysical S-factor and thermonuclear reaction rates for (p,n) medium elements reactions. *Journal of Physics: Conference Series*, 1660(1):012102, 2020.

[107] M. Ueda, A. J. Sargeant, M. P. Pato, and M. S. Hussein. Evaluation of effective astrophysical S factor for non-resonant reactions. *Progress of Theoretical Physics Supplement*, 146:634–635, 2002.

[108] M. Ueda, A. J. Sargeant, M. P. Pato, and M. S. Hussein. Resonances and thermonuclear reaction rates for charged particle collisions. *Physical Review C*, 70(2), 2004.

[109] M. Beard, A. V. Afanasjev, L. C. Chamon, L. R. Gasques, M. Wiescher, and D. G. Yakovlev. Astrophysical S factors for fusion reactions involving C, O, Ne, and Mg isotopes. *Atomic Data and Nuclear Data Tables*, 96(5):541–566, 2010.

[110] J. T. Huang, C. A. Bertulani, and V. Guimarães. Radiative capture of nucleons at astrophysical energies with single-particle states. *Atomic Data and Nuclear Data Tables*, 96(6):824–847, 2010.

[111] E. G. Adelberger, A. García, R. G. Robertson, K. A. Snover, A. B. Balantekin, K. Heeger, M. J. Ramsey-Musolf, D. Bemmerer, A. Junghans, C. A. Bertulani, and et al. Solar fusion cross sections. II. The pp chain and CNO cycles. *Reviews of Modern Physics*, 83(1):195–245, 2011.

[112] G. V. Rossum and F. L. Drake. *Python 3: Reference Manual*. SohoBooks, 2009.

[113] W. McKinney. *9th Python in Science Conference*, page 56–61. Scipy, 2010. Editors Stéfan van der Walt and Jarrod Millman.

[114] C. R. Harris, K. J. Millman, S. J. van der Walt, R. Gommers, P. Virtanen, D. Cournapeau, E. Wieser, J. Taylor, S. Berg, N. J. Smith, and et al. Array programming with NumPy. *Nature*, 585(7825):357–362, 2020.

[115] P. Virtanen, R. Gommers, T. E. Oliphant, M. Haberland, T. Reddy, D. Cournapeau, E. Burovski, P. Peterson, W. Weckesser, J. Bright, and et al. Scipy 1.0: Fundamental algorithms for scientific computing in Python. *Nature Methods*, 17(3):261–272, 2020.

[116] J. D. Hunter. Matplotlib: A 2D Graphics Environment. *Computing in Science & Engineering*, 9(3):90–95, 2007.

[117] P. Descouvemont, A. Adahchour, C. Angulo, A. Coc, and E. Vangioni-Flam. Compilation and R-matrix analysis of Big Bang nuclear reaction rates. *Atomic Data and Nuclear Data Tables*, 88(1):203–236, 2004.

[118] Y. Xu, K. Takahashi, S. Goriely, M. Arnould, M. Ohta, and H. Utsunomiya. NACRE II: an update of the NACRE compilation of charged-particle-induced thermonuclear reaction rates for nuclei with mass number $A < 16$. *Nuclear Physics A*, 918:61–169, 2013.

[119] V. V. Zerkin, B. Pritychenko, J. Totans, L. Vrapcenjak, A. Rodionov, and G. I. Shulyak. EXFOR-NSR PDF database: A system for nuclear knowledge preservation and data curation. *Journal of Instrumentation*, 17(03), 2022.

[120] O. Iwamoto, N. Iwamoto, K. Shibata, A. Ichihara, S. Kunieda, F. Minato, and S. Nakayama. Status of JENDL. *EPJ Web of Conferences*, 239:09002, 2020.

[121] V. M. Bystritsky, V. V. Gerasimov, A. R. Krylov, S. S. Parzhitskii, G. N. Dudkin, V. L. Kaminskii, B. A. Nechaev, V. N. Padalko, A. V. Petrov, G. A. Mesyats, and et al. Study of the pd reaction in the astrophysical energy region using the Hall accelerator. *Nuclear Instruments and Methods in Physics Research Section A: Accelerators, Spectrometers, Detectors and Associated Equipment*, 595(3):543–548, 2008.

[122] G. J. Schmid, R. M. Chasteler, C. M. Laymon, H. R. Weller, R. M. Prior, and D. R. Tilley. Polarized proton capture by deuterium and the ^{2}H(p, γ)^{3}He astrophysical S factor. *Physical Review C*, 52(4), 1995.

[123] B. L. Berman, L. J. Koester, and J. H. Smith. Photodisintegration of He^3. *Physical Review*, 133(1B), 1964.

[124] J. B. Warren, K. L. Erdman, L. P. Robertson, D. A. Axen, and J. R. Macdonald. Photodisintegration of He^3 near the Threshold. *Physical Review*, 132(4):1691–1692, 1963.

[125] U. Greife, F. Gorris, M. Junker, C. Rolfs, and D. Zahnow. Oppenheimer-Phillips effect and electron screening in $d+d$ fusion reactions. *Zeitschrift für Physik A Hadrons and Nuclei*, 351(1):107–112, 1995.

[126] A. Krauss, H. W. Becker, H. P. Trautvetter, C. Rolfs, and K. Brand. Low-energy fusion cross sections of D + D and D + ^{3}He reactions. *Nuclear Physics A*, 465(1):150–172, 1987.

[127] D. S. Leonard, H. J. Karwowski, C. R. Brune, B. M. Fisher, and E. J. Ludwig. Precision measurements of precision measurements of ^{2}H(d, p)^{3}H and ^{2}H(d, n)^{3}He total cross sections at Big Bang nucleosynthesis energies. *Physical Review C*, 73(4), 2006.

[128] R. L. Schulte, M. Cosack, A. W. Obst, and J. L. Weil. ^{2}H + reactions from 1.96 to 6.20 MeV. *Nuclear Physics A*, 192(3):609–624, 1972.

[129] A. Tumino, C. Spitaleri, A. M. Mukhamedzhanov, S. Typel, M. Aliotta, V. Burjan, M. Gimenez del Santo, G. G. Kiss, V. Kroha, Z. Hons, and et al. Low-energy d + d fusion reactions via the Trojan Horse method. *Physics Letters B*, 700(2):111–115, 2011.

[130] C. Casella, H. Costantini, A. Lemut, B. Limata, R. Bonetti, C. Broggini, L. Campajola, P. Corvisiero, J. Cruz, A. D'Onofrio, and et al. First measurement of the d(p, γ)^{3}He cross section down to the solar Gamow peak. *Nuclear Physics A*, 706(1-2):203–216, 2002.

[131] V. N. Fetisov, A. N. Gorbunov, and A. T. Varfolomeev. Nuclear photoeffect on three-particle nuclei. *Nuclear Physics*, 71(2):305–342, 1965.

[132] K. N. Geller, E. G. Muirhead, and L. D. Cohen. The ^{2}H(p, γ)^{3}He reaction at the breakup threshold. *Nuclear Physics A*, 96(2):397–400, 1967.

[133] G. M. Griffiths, E. A. Larson, and L. P. Robertson. The capture of protons by deuterons. *Canadian Journal of Physics*, 40(4):402–411, 1962.

[134] L. Ma, H. J. Karwowski, C. R. Brune, Z. Ayer, T. C. Black, J. C. Blackmon, E. J. Ludwig, M. Viviani, A. Kievsky, R. Schiavilla, and et al. Measurements of ^{1}H($\vec{d}$, γ)^{3}He and ^{2}H($\vec{p}$, γ)^{3}He at very low energies. *Physical Review C*, 55(2):588–596, 1997.

[135] G. J. Schmid, M. Viviani, B. J. Rice, R. M. Chasteler, M. A. Godwin, G. C. Kiang, L. L. Kiang, A. Kievsky, C. M. Laymon, R. M. Prior, and et al. Effects of Non-nucleonic Degrees of freedom in the D($\vec{p}$, γ)^{3}He and p($\vec{d}$, γ)^{3}He Reactions. *Physical Review Letters*, 76(17):3088–3091, 1996.

[136] W. Wölfli, R. Bösch, J. Lang, R. Müller, and P. Marmier. Einfang von Protonen durch Deuteronen. *Helvetica Physica Acta*, 40:946–972, 1967.

[137] L. T. Baby, C. Bordeanu, G. Goldring, M. Hass, L. Weissman, V. N. Fedoseyev, U. Köster, Y. Nir-El, G. Haquin, H. W. Gäggeler, R. Weinreich, and et al. New measurement of the proton capture rate on ^{7}Be and the $S_{17}(0)$ factor. *Physical Review C*, 67(6), 2003.

[138] A. R. Junghans, E. C. Mohrmann, K. A. Snover, T. D. Steiger, E. G. Adelberger, J. M. Casandjian, H. E. Swanson, L. Buchmann, S. H. Park, A. Zyuzin, and et al. Precise measurement of the ^{7}Be(p, γ)^{8}B S factor. *Physical Review C*, 68(6), 2003.

[139] A. R. Junghans, K. A. Snover, E. C. Mohrmann, E. G. Adelberger, and L. Buchmann. Updated S factors for the ^{7}Be(p, γ)^{8}B reaction. *Physical Review C*, 81(1), 2010.

[140] F. Schümann, S. Typel, F. Hammache, K. Sümmerer, F. Uhlig, I. Böttcher, D. Cortina, A. Förster, M. Gai, H. Geissel, and et al. Low-energy cross section of the ^{7}Be(p, γ)^{8}B solar fusion reaction from the Coulomb dissociation of ^{8}B. *Physical Review C*, 73(1), 2006.

[141] J. D. King, R. E. Azuma, J. B. Vise, J. Görres, C. Rolfs, H. P. Trautvetter, and A. E. Vlieks. Cross section and astrophysical S-factor for the ^{13}C(p, γ)^{14}N reaction. *Nuclear Physics A*, 567(2):354–376, 1994.

[142] E. J. Woodbury and W. A. Fowler. The Cross Section for the Radiative Capture of Protons by C^{13} at 129 kev. *Physical Review*, 85(1):51–57, 1952.

[143] H. W. Becker, K. U. Kettner, C. Rolfs, and H. P. Trautvetter. The ^{12}C + ^{12}C reaction at subcoulomb energies (II). *Zeitschrift für Physik A Atoms and Nuclei*, 303(4):305–312, 1981.

[144] G. Fruet, S. Courtin, M. Heine, D. G. Jenkins, P. Adsley, A. Brown, R. Canavan, W. N. Catford, E. Charon, D. Curien, and et al. Advances in the Direct Study of Carbon Burning in Massive Stars. *Physical Review Letters*, 124(19), 2020.

[145] T. Spillane, F. Raiola, C. Rolfs, D. Schürmann, F. Strieder, S. Zeng, H.-W. Becker, C. Bordeanu, L. Gialanella, M. Romano, and et al. ^{12}C + ^{12}C Fusion Reactions near the Gamow Energy. *Physical Review Letters*, 98(12), 2007.

[146] W. P. Tan, A. Boeltzig, C. Dulal, R. J. deBoer, B. Frentz, S. Henderson, K. B. Howard, R. Kelmar, J. J. Kolata, J. Long, and et al. New Measurement of ^{12}C + ^{12}C Fusion Reaction at Astrophysical Energies. *Physical Review Letters*, 124(19), 2020.

[147] H. Spinka and H. Winkler. Experimental determination of the total reaction cross section of the stellar nuclear reaction ^{16}O + ^{16}O. *Nuclear Physics A*, 233(2):456–494, 1974.

[148] R. Buompane, A. Di Leva, L. Gialanella, A. D'Onofrio, M. De Cesare, J. G. Duarte, Z. Fülöp, L. R. Gasques, G. Gyürky, L. Morales-Gallegos, and et al. Determination of the ^{7}Be(p, γ)^{8}B cross section at astrophysical energies using a radioactive ^{7}Be ion beam. *Physics Letters B*, 824:136819, 2022.

[149] D. Gaspard. Connection formulas between Coulomb wave functions. *Journal of Mathematical Physics*, 59(11):112104, 2018.

[150] L. C. Chamon, B. V. Carlson, and L. R. Gasques. São Paulo potential version 2 (SPP2) and Brazilian nuclear potential (BNP). *Computer Physics Communications*, 267:108061, 2021.

[151] A. Diaz-Torres. OWL: A code for the two-center shell model with spherical Woods–Saxon potentials. *Computer Physics Communications*, 224:381–386, 2018.

[152] I. I. Gontchar and M. V. Chushnyakova. DFMSPH14: A C-code for the double folding interaction potential of two spherical nuclei. *Computer Physics Communications*, 206:97–102, 2016.

[153] P. Descouvemont. An R-matrix package for coupled-channel problems in nuclear physics. *Computer Physics Communications*, 200:199–219, 2016.

[154] I. J. Thompson, R. J. deBoer, P. Dimitriou, S. Kunieda, M. T. Pigni, G. Arbanas, H. Leeb, T. Srdinko, G. Hale, P. Tamagno, and et al. Verification of R-matrix calculations for charged-particle reactions in the resolved resonance region for the ^{7}Be system. *The European Physical Journal A*, 55(6), 2019.

[155] R. E. Azuma, E. Uberseder, E. C. Simpson, C. R. Brune, H. Costantini, R. J. de Boer, J. Görres, M. Heil, P. J. LeBlanc, C. Ugalde, and et al. Azure: An *R*-matrix code for nuclear astrophysics. *Physical Review C*, 81(4), 2010.

[156] F. Salvat and J. M. Fernández-Varea. RADIAL: A Fortran subroutine package for the solution of the radial Schrödinger and Dirac wave equations. *Computer Physics Communications*, 240:165–177, 2019.

[157] K. Hagino, N. Rowley, and A. T. Kruppa. A program for coupled-channel calculations with all order couplings for heavy-ion fusion reactions. *Computer Physics Communications*, 123(1-3):143–152, 1999.